THE $^{16}O(\alpha,\gamma)^{20}Ne$ AND $^{28}Si(\alpha,\gamma)^{32}S$ REACTIONS AT LOW ENERGY

Thesis by

James Waldo Toevs

In Partial Fulfillment of the Requirements

For the Degree of

Doctor of Philosophy

California Institute of Technology

Pasadena, California

1970

(Submitted December 30, 1969)

This thesis is dedicated to my wife, Lois, who at once fulfilled the responsibilities of mother and scientist, and still gave a wife's compassion and love.

ACKNOWLEDGMENTS

It is with pleasure that the author acknowledges the friendly, stimulating atmosphere of the Kellogg Radiation Laboratory, and thanks its entire staff for their assistance and support.

In particular, the continued encouragement and guidance of Professors W. A. Fowler and C. A. Barnes is sincerely appreciated. Professor Fowler suggested the experiments and provided insight into their astrophysical motivation, and Professor Barnes shared his fine knowledge of the intricacies of experimental physics.

The friendship and help of Dr. Peter B. Lyons, my associate through several years of research, and his invaluable assistance with the investigation of the $^{16}O(\alpha,\gamma)^{20}Ne$ reaction, are gratefully acknowledged.

Calibration of the original spectrometer was carried out in collaboration with Dr. Lyons and Dr. D. G. Sargood. The assistance of Mr. Kendahl Shane in measuring the $^{28}Si(\alpha,\gamma)^{32}S$ yield is also acknowledged.

Thanks for financial support are given for a National Defense Education Act Fellowship, and Graduate Research and Teaching Assistantships from the California Institute of Technology. The research was supported in part by the Office of Naval Research (Nonr-220(47)) and the National Science Foundation (GP-9114).

(ACKNOWLEDGMENTS--continued)

Special thanks are extended to several members of my family:

To my grandfather, Mr. John D. Mills, for his patient and joyful response to a little boy's endless questions;

To my parents, Mr. and Mrs. Waldo C. Toevs, for their love, and their examples of dedication and integrity;

To my wife, Dr. Lois Toevs, to whom this thesis is dedicated;

And to my little daughter, Kimberly Erin, who provided such delightful distraction during the preparation of the thesis.

ABSTRACT

The $^{28}Si(\alpha,\gamma)^{32}S$ and $^{16}O(\alpha,\gamma)^{20}Ne$ reactions have been investigated to provide data for the calculation of the stellar rates of these reactions. The gamma rays were counted with a NaI(Tl) detection system having a high detection efficiency which is approximately independent of the gamma-ray cascade structure of a nuclear level; the detection efficiency was determined experimentally. The reaction $^{28}Si(\alpha,\gamma)^{32}S$ was studied for He^{+} bombarding energies from 1.4 to 2.7 MeV, and in this region, five new resonances were found, and their strengths, $(2J+1)\Gamma_{\alpha}\Gamma_{\gamma}/\Gamma$, were measured. An upper limit for the cross section has also been established for bombarding energies below 1.7 MeV. The $^{16}O(\alpha,\gamma)^{20}Ne$ reaction was investigated in the energy region from 0.85 to 1.8 MeV; strengths for the previously known resonances were measured, and an upper limit for the cross section was determined for energies below 1 MeV. Stellar interaction rates and photodisintegration rates have been calculated from the measured resonance strengths, and semi-empirical fits to these rates have been given to facilitate astrophysical calculations.

TABLE OF CONTENTS

TABLE OF CONTENTS (continued)

TABLE OF CONTENTS (continued)

LIST OF FIGURES

LIST OF TABLES

I. INTRODUCTION

A. Astrophysical Situation

The realization that nuclear reactions must be the primary energy sources in stars suggests that stellar processes play a fundamental role in the creation of the chemical elements. It is evident that a study of stellar processes will require nuclear parameters that can be provided only by experimental nuclear physics. The Kellogg Radiation Laboratory has for many years directed much effort toward specific problems of interest to the study of stellar evolution and nucleosynthesis; this investigation is another effort in this tradition.

The motivation for the present experimental study was provided several years ago when Fowler and Hoyle (1964) discussed the α- and e-processes (Burbidge, Burbidge, Fowler, and Hoyle, 1957), for a highly evolved star with a silicon core. It is now widely accepted that carbon and oxygen burning convert the core primarily to ^{32}S, with traces of other elements. Further contraction and heating thermally photodisintegrate the ^{32}S to ^{28}Si, which is the most refractory (tightly bound) nucleus in this mass region. The high Coulomb barrier prevents ^{28}Si from reacting with itself, so that the next nuclear burning stage, beginning at a temperature near 3×10^9 °K, involves the photodisintegration of the ^{28}Si. The protons, α-particles, and neutrons liberated in the silicon photodisintegration, quickly combine with other ^{28}Si nuclei to produce heavier nuclei, eventually building up to the iron group elements.

Bodansky, Clayton, and Fowler (1968) introduced the idea of "quasi-equilibrium", which unified the α- and e-processes into a single process, now referred to as silicon burning. Because the ^{28}Si photodisintegration proceeds quite slowly, relative to the other nuclear reactions taking place, a series of reactions involving heavier nuclei come into equilibrium, such as

$$^{28}Si + \alpha \rightleftharpoons {}^{32}S + \gamma$$

$$^{32}S + \alpha \rightleftharpoons {}^{36}Ar + \gamma$$

and so on. For reactions in equilibrium, the number densities, N_i, of the constituents, are related by the statistical Saha equation (Clayton, 1968). For the reaction, $0 + 1 \rightleftharpoons 2 + \gamma$, this is

$$\frac{N_0 N_1}{N_2} = \frac{(2\pi\mu kT)^{3/2}}{h^3} \frac{G_0 G_1}{G_2} \exp(-Q/kT) \qquad (1)$$

where μ is the reduced mass of 0 and 1, the G_i are the nuclear partition functions, h is Planck's constant, and Q is the energy release in the forward direction. Note that the relative abundances do not depend on detailed knowledge of the reaction cross section when the reaction is in equilibrium. Fundamental to the quasi-equilibrium model is the fact that the photodisintegration lifetimes for $A > 28$ nuclei are much shorter than the ^{28}Si lifetime, so that the number densities, N_i, in Eq. 1 are effectively constant for periods long compared with the lifetimes of the $A > 28$ nuclei.

Bodansky et al. (1968) and Truran, Cameron, and Gilbert (1966) have calculated that, although the photodisintegration

rate of ^{24}Mg, $\lambda_\gamma(^{24}Mg)$, is faster than $\lambda_\gamma(^{28}Si)$, the equilibrium concentration of ^{24}Mg is much less than that of ^{28}Si, so

$$\lambda_\gamma(^{28}Si)N(^{28}Si) \gg \lambda_\gamma(^{24}Mg)N(^{24}Mg),$$

and the reaction, $^{28}Si + \gamma \rightleftarrows {}^{24}Mg + \alpha$ also comes into equilibrium. Therefore, the ^{24}Mg photodisintegration lifetime determines the time scale for the silicon burning process. It then follows that the only necessary nuclear parameters, for the quasi-equilibrium approximation, are the various reaction Q values, and the $^{20}Ne(\alpha,\gamma)^{24}Mg$ cross section, which is thought to dominate the ^{24}Mg photodisintegration. This cross section has been studied by Smulders (1965) for 1.2 MeV $< E_{He^+} <$ 3.2 MeV, and is being investigated at lower energies in Kellogg Laboratory.

Bodansky et al. (1968) point out that, although the above model successfully accounts for the abundances of many of the elements having $28 < A < 56$, the silicon burning stage may be truncated in such a way that the final abundances could not be calculated on the basis of quasi-equilibrium. An example would be an explosive process, in which the resulting expansion might so quickly cool the system that the photodisintegration lifetimes would become long compared with the time scale involved. In such a "freeze out," knowledge of the (α,γ), (p,γ), and (n,γ) cross sections on each nucleus would be required to calculate the final abundances. The $^{28}Si(\alpha,\gamma)^{32}S$ reaction is of interest for this reason. Explosive processes have been discussed by Arnett (1969), Truran and Arnett (1969), Truran, Cameron, and Gilbert

(1966), Truran, Arnett, and Cameron (1967), and Wagoner (1969).

The reaction $^{16}O(\alpha,\gamma)^{20}Ne$ is also of interest in silicon burning in that the photodisintegration of ^{20}Ne is one link in the reaction chain $^{28}Si \rightarrow 7\ ^{4}He$, which supplies the α particles necessary for element synthesis in silicon burning. At these high temperatures, however, the ^{20}Ne lifetime is so much shorter than the ^{24}Mg lifetime that the reaction cross section is not usually too important to stellar model calculations. The cross section is important, however, in determining the nuclear abundances at the end of helium burning, which occurs at much lower temperatures ($\approx 10^{8}$ ^{o}K). This process begins with the reaction, $3\ ^{4}He \rightarrow {}^{12}C + \gamma$, followed by $^{12}C(\alpha,\gamma)^{16}O$, presently being studied in Kellogg Laboratory, and then perhaps followed by $^{16}O(\alpha,\gamma)^{20}Ne$ and $^{20}Ne(\alpha,\gamma)^{24}Mg$. That the abundance of ^{20}Ne is so large is not yet understood, for the $^{16}O(\alpha,\gamma)^{20}Ne$ reaction rate, based on presently available knowledge, is too slow to produce much neon, and any neon produced should be consumed by the more rapid $^{20}Ne(\alpha,\gamma)^{24}Mg$ reaction.

$^{16}O(\alpha,\gamma)^{20}Ne$ could also be of significance in the "helium flash," discussed by Hayashi, Hoshi, and Sugimoto (1962), which is thought to accompany the onset of helium burning in a degenerate core. Asano and Sugimoto (1968) have proposed the following model to explain the linear relationship between metal abundance and absolute magnitude in horizontal branch stars.

The luminosity due to a helium burning core is determined by the mass of the core, which is fixed at the time of the helium flash. The timing of the flash and the core properties are determined primarily by the abundance of heavy elements ($A > 10$), and by hydrogen burning in the shell. The shell burning depends on the hydrogen and helium concentrations in the shell source itself (Faulkner, 1966). It has been shown that mixing into the shell source does not occur during the helium flash (Hayashi et al., 1962), so that the original hydrogen and helium abundances in a helium burning star may be obtained from knowledge of the star's luminosity, provided that the luminosity is due primarily to helium burning, not shell hydrogen burning. It follows that the study of an extreme population II star, in the helium burning stage, could yield the primordial helium abundance, which is difficult to determine directly.

Asano and Sugimoto then propose that the heavy elements, particularly ^{14}N, may trigger the helium flash at a somewhat earlier temperature, through the reaction $^{14}N(\alpha,\gamma)^{18}F$, and that this temperature is directly related to the ^{14}N concentration in the core. Since the total concentration of carbon, nitrogen, and oxygen (X_{CNO}) remains constant during CNO burning, the core nitrogen abundance may be inferred from spectroscopic observations of the stellar surface. This, in brief, is the mechanism proposed by Asano and Sugimoto (1968) to explain the metal-magnitude relationship mentioned above.

A problem arises, however, with regard to the reaction rate for $^{14}N(\alpha,\gamma)^{18}F$, which Asano and Sugimoto had taken from Reeves (1965). More recent data (Olness and Warburton, 1967; Parker, 1968)

has shown the actual rate to be at least 3000 times slower than the rate quoted by Reeves; therefore $^{14}N(\alpha,\gamma)^{18}F$ could not trigger the flash soon enough for this mechanism to work.

Fowler (1969) suggested that the $^{16}O(\alpha,\gamma)^{20}Ne$ reaction might do the job if an as yet undetected, low-energy resonance existed, which is further motivation for the present study.

B. Astrophysically Motivated Experimental Considerations

The gamma ray detection system used in the following measurements is a slightly modified version of a system which was developed several years ago in the hope that it could be used to study various reactions important to the silicon burning process. The earlier system was used to measure the $^{27}Al(p,\gamma)^{28}Si$ and $^{24}Mg(\alpha,\gamma)^{28}Si$ reactions (Lyons, 1969, hereafter referred to as PBL; Lyons, Toevs, and Sargood, 1969, hereafter referred to as LTS). Although the spectrometer was described in detail in PBL and LTS, its applicability to other astrophysical reactions warrants a discussion here of the astrophysical requirements for such a system. The effects of the modifications will be discussed in a later section.

An astrophysical interest in particle-capture yield measurements affects the philosophy of the experiment in several ways, which are more easily described with a look at the relevant stellar interaction rate equation. Clayton (1968) derives the following formula for the stellar rate, which is the product of cross section and velocity averaged over a Maxwell-Boltzmann distribution, for a region in which the nuclear reaction in question is dominated by resonances:

$$\langle \sigma v \rangle = \left[\frac{2\pi\hbar^2}{\mu kT}\right]^{3/2} \sum_r \frac{\omega \Gamma_0 \Gamma_\gamma}{\hbar \Gamma}_r \exp(-E_r/kT) \qquad (2)$$

in which E_r is the center-of-mass energy for the r^{th} resonance, $\omega\Gamma_0\Gamma_\gamma/\Gamma$ is the resonance strength for the r^{th} resonance (this will be discussed later), Γ_0 is the proton or alpha particle width for that resonance, and the other symbols have the same meanings they had in Eq. 1. In resonance-dominated regions, the non-resonant or between-resonanceyield is thought to come from the tails of the Breit-Wigner resonances, and so is accounted for in Eq. 2. Using the principle of detailed balance, the corresponding equation for the photodisintegration rate is obtained for the reaction $\gamma + 2 \rightarrow 0 + 1$,

$$\lambda_{\gamma,0} = \frac{(2J_0+1)(2J_1+1)}{G_2} \left[\frac{\mu kT}{2\pi\hbar^2}\right]^{3/2} \langle \sigma v \rangle \exp(-Q/kT) \qquad (3)$$

In the stellar situation, the probability of the decay of a level by gamma emission could be enhanced by induced emission, effectively changing the value of Γ_γ from the value measured in the laboratory. This problem requires a look at the temperatures and energies involved. For the helium burning process, the temperature range is $5\text{-}15 \times 10^7$ °K, and the corresponding thermal energy range, kT, is 4.3-12.9keV. The silicon burning ranges are $1\text{-}5 \times 10^9$ °K and 86-430 keV. The energy level diagrams for the compound nuclei to be investigated are shown in Figures 1 and 2. These diagrams show that the Q value for the $^{28}Si(\alpha,\gamma)^{32}S$ reaction is 6.95 MeV. Typical excitation energies for the reactions of interest in silicon burning are 8-15 MeV, and, since the first transition in a cascade

FIGURE 1: Energy Level Diagram of ^{32}S

The energies, spins, and parities for the ^{32}S levels, and the threshold energies for $^{28}Si + \alpha$ and $^{31}P + p$ were taken from the compilation of Endt and Van der Leun (1967). The energy range investigated in the present work is indicated.

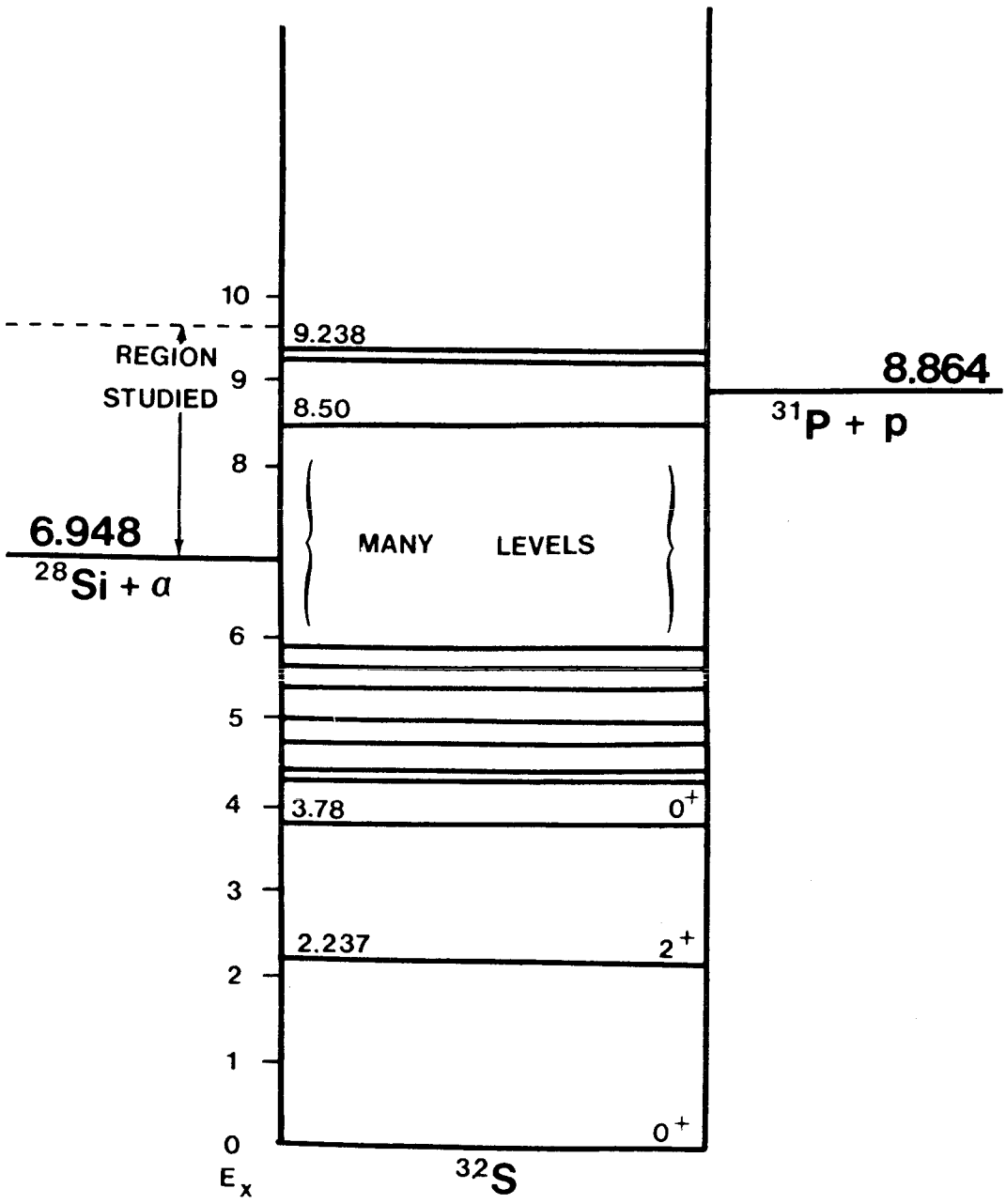
10
9.238
REGION
STUDIED
9
8.50
8
MANY LEVELS
6.948
28Si + α
6
5
4
3.78
0+
3
2.237
2+
2
1
0+
0
Ex
32S
8.864
31P + p

FIGURE 2: Energy Level Diagram of ^{20}Ne

The energies, spins, and parities for the ^{20}Ne levels, and the threshold energy for $^{16}O + \alpha$, were taken from the compilation of Ajzenberg-Selove and Lauritsen (1959), and from Kuehner (1961) and Gove et al.(1961). The energy range covered in the present study extended from the $^{16}O + \alpha$ threshold to the top of the diagram.

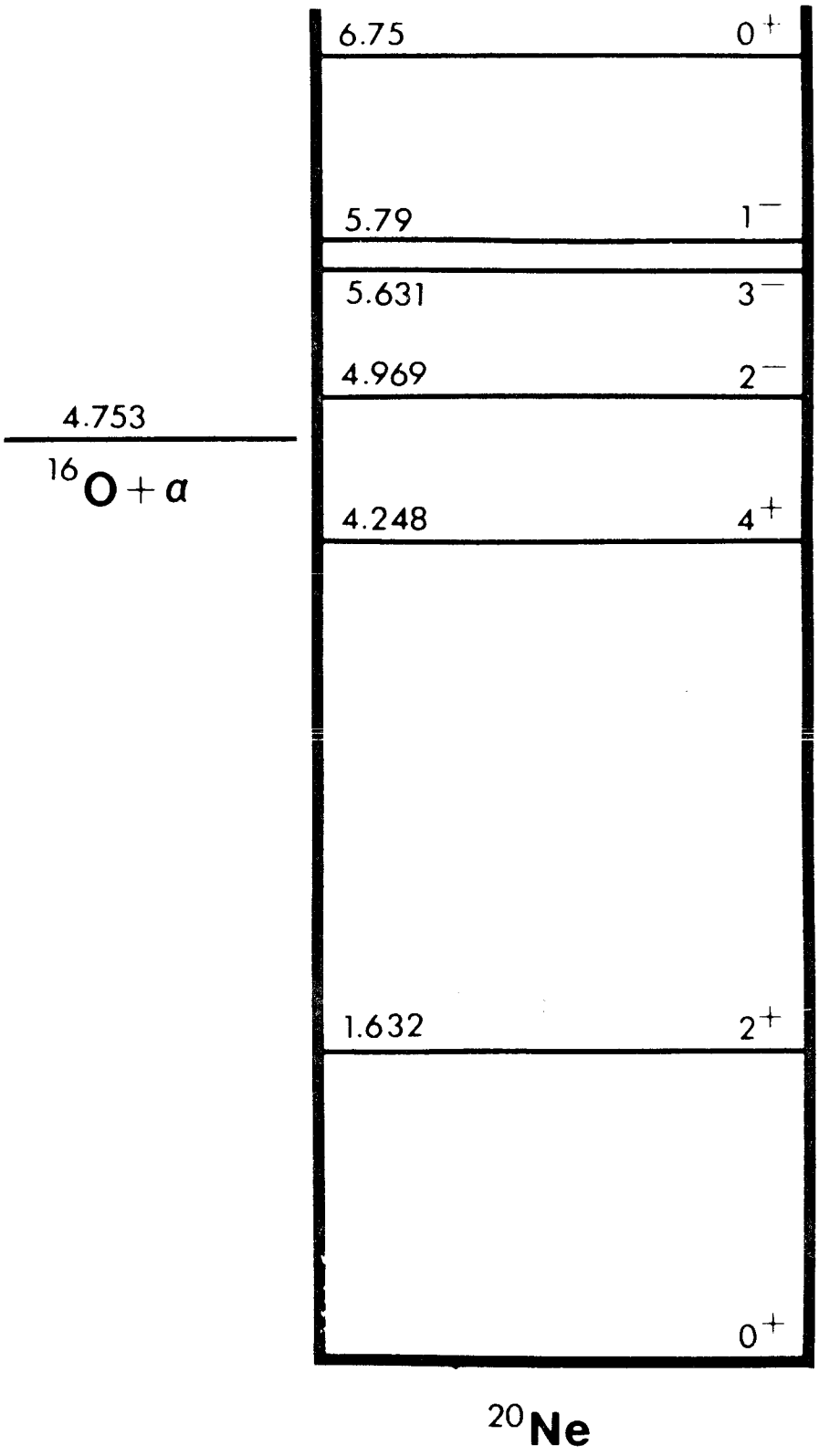
6.75
0+
5.79
1−
5.631
3−
4.969
2−
4.753
16O + a
4.248
4+
1.632
2+
0+
20Ne

is invariably to a relatively low-lying state, induced emission from the excited nucleus is weak and can be ignored. The $^{16}O(\alpha,\gamma)^{20}Ne$ excitation energies are lower, but the temperature range for helium burning is so much lower that induced emission is clearly negligible.

Comparing the thermal energies and excitation energies, one sees immediately that the exponential factor, $\exp(-E_r/kT)$, will cause low energy resonances to be extremely important, if not dominant, in the stellar situation. This poses a problem to the experimenter, because, at low energies, the formation of the resonance is inhibited by the Coulomb barrier. The gamma ray spectrometer, then, must possess a high detection efficiency so that low yield resonances may be observed, and it must also have high enough resolution to allow discrimination between the γ rays of interest and γ rays and neutrons produced in contaminant reactions.

The high excitation energies encountered in silicon-burning reactions cause one to expect complicated cascade structure in the decays from the high levels in the compound nucleus. As can be seen from Equation 2, a calculation of the interaction rate requires the total γ ray width, Γ_γ, implying that the different γ transitions from a given level are not weighted differently by the stellar environment. For the particle capture case, this is clearly so, because induced emission can be neglected, and because the processes of pair emission and internal conversion, which could be affected by the stellar environment, are extremely weak processes for light

nuclei. For the case of photodisintegration, the level in question may be created by further excitation of a thermally excited state, but the thermodynamic probability for such multiple excitations is the same as for direct excitation from the ground state, since the excitation energies are so high that the thermal factor for the γ rays involved is given accurately by $\exp(-E_\gamma/kT)$.

The gamma spectrometer therefore must treat cascades in one of the following ways: it can require a detailed knowledge of the cascade structure, from which the detection efficiency for the cascade can be obtained, but from which no additional knowledge of astrophysical interest can be derived; or it can be used in such a way that its detection efficiency is independent of the cascade structure. This second method requires a spectrum of less accurate detail, since branching ratios for the cascades are not needed; in view of the very low yield to be expected from some of the resonances of interest, the second approach seems more widely useful.

C. Determining the Resonance Strength

Equation 2 contains an expression for the resonance strength, $\omega\Gamma_0\Gamma_\gamma/\Gamma$, in which $\omega = (2J_r + 1)/(2J_0 + 1)(2J_1 + 1)$. In the literature, one may find this expression and the similar expression, $(2J_r + 1)\Gamma_0\Gamma_\gamma/\Gamma$, both referred to as the resonance strength. For the reactions studied here, J_0 and J_1 are zero, so the distinction is academic; for consistency, the term resonance strength will refer to the latter form.

The resonance strength must be extracted from the available experimental information, which includes the beam energy; the total number of incident particles, N_0; the total number of times that the resonant level decayed by gamma emission, N_γ (from the observed spectrum for the resonance and knowledge of the detection efficiency of the system); and properties of the target, such as the number of target nuclei per cm^3, n_1.

By incorporating the familiar concept of cross section, σ (cm^2), the yield at an energy, E, may be expressed simply as the product of the number of incident nuclei, the number of target nuclei per unit area seen by the incident nuclei, and the cross section. In practice, the yield will involve an integral over all of the incident particle energies for which $\sigma(E-E_r)$, near the resonance at E_r, is non-negligible. The Breit-Wigner shape of $\sigma(E-E_r)$ for a single resonance will be discussed shortly. The targets used for this experiment were "thick" targets, that is, the beam energy lost in traveling through the target, ΔE, was large compared with the instrumental beam resolution, and with the energy range for which $\sigma(E-E_r)$ is not small. Therefore, for incident beam energies well above E_r, yet low enough that $E_r-\Delta E$ is well below E_r, the following statements are valid:

(1) The energy integral mentioned above may be extended to cover all energies (this is simply assuming that the target is infinitely thick).

(2) The number of target nuclei/cm^2 that a particle in the target will see, if its energy is between E and E + dE, is

$$\frac{n_1 dE}{(dE/dx)} .$$

(3) For the narrow resonances expected in this study, it may be assumed that dE/dx is constant over the energy range for which $\sigma(E-E_r)$ contributes to the integral.

With these considerations, the yield may be written

$$N_\gamma = \frac{N_0}{\mathcal{E}(E_r)} \int \sigma(E-E_r)dE \qquad (4)$$

where

$$\mathcal{E}(E_r) = \frac{1}{n_1}\left(\frac{dE}{dx}\right)_{E_r} ,$$

and is called the stopping power per atom of the target. For a compound target, the value of $(dE/dx)_{Er}$ for the compound must be used. Stopping power values for the silicon and oxygen in the targets used in this study were taken from Williamson and Boujot (1962), and Whaling (1958), respectively.

As the beam energy is varied from below E_r to well above E_r, the resonance yield will appear as a step, whose front edge shape will depend on the shapes of $\sigma(E-E_r)$ and the instrumental resolution. The midsection of the step will appear as a flat plateau, since, from Equation 4, the yield in this region is independent of the beam energy. The shape of the trailing edge ($E>E_r$) will be determined by the instrumental resolution, $\sigma(E-E_r)$, and the straggling

of the beam in the target. Because of the straggling contribution, the trailing edge of the step will be broader than the leading edge. Note that in the plateau region, described by Equation 4, specific functions describing the instrumental resolution and the beam profile (related to straggling) in the target, are not required. This is fortunate, because these functions are usually difficult to determine.

A completely general formula for the yield in any target situation is discussed by Gove (1959).

For a single, isolated resonance, the cross section is given by the Breit-Wigner formula,

$$\sigma(E_{CM}) = \pi \lambda^2 \frac{(2J_r + 1)}{(2J_0 + 1)(2J_1 + 1)} \frac{\Gamma_0 \Gamma_\gamma}{(E_{CM} - E_{r,CM})^2 + (\Gamma/2)^2} \quad (5)$$

in which:

E_{CM} is the beam energy in the center-of-mass system, equal to $EA_1/(A_0+A_1)$, where E is the lab energy, and A_0 and A_1 are the masses of 0 and 1, the incident and target nuclei;

$E_{r,CM}$ is the resonance energy in the center-of-mass system;

$\lambda^2 = \hbar^2/2\mu E_{CM}$, where, as before, μ is the reduced mass of 0 and 1;

J_0, J_1, and J_r are the spins of 0, 1, and the resonant level;

Γ_0, Γ_γ, and Γ are the widths of the incident particle channel, total electromagnetic width, and total resonance width, all in center-of-mass units.

Inserting this form for σ into Equation 4, integrating, and

solving for the resonance strength, one obtains

$$(2J_r + 1)(\Gamma_0\Gamma_\gamma/\Gamma)_{CM} = \left[\frac{A_1}{A_0+A_1}\right]^3 \frac{M_0 E_r \epsilon(E_r)(2J_0 + 1)(2J_1 + 1)}{\hbar^2\pi^2} \frac{N_\gamma}{N_0} \qquad (6)$$

where M_0 is the mass of the incident particle. Note that E_r is in laboratory units, and that the subscript "CM" indicates that the resonance strength is given in the center-of-mass system, which is appropriate for astrophysical calculations.

D. State of Previous Knowledge

The $^{28}Si(\alpha,\gamma)^{32}S$ reaction has been studied by Smulders (1964), using a natural silicon target, for He^+ bombarding energies from 2.1 to 3.3 MeV. Four resonances were found, at energies of 2.618, 2.878, 2.904, and 3.162 MeV, all $\pm$ 4 keV. The resonance strengths were measured, and the spins and parities of the levels were determined. A very weak resonance at 2.183 MeV, was reported by Smulders in an earlier reference (Endt and Van der Leun, 1962), but could not be confirmed in the 1964 paper.

Langevin, Laurent, and Vernotte (1965) studied the reaction on a natural silicon target for bombarding energies from 3.2 to 4.3 MeV. Nine resonances were found, and spins and parities were determined for four of these. The strengths were not measured.

Cross sections for the three known, astrophysically important resonances in $^{16}O(\alpha,\gamma)^{20}Ne$ have been measured by Van der Leun,

Sheppard, and Smulders (1965). The laboratory energies of these resonances are 1.116, 1.319, and 2.490 MeV, and the corresponding excitations in ^{20}Ne are 5.631, 5.808, and 6.745 MeV. Pearson (1963) has measured cross sections for resonances between 4.8 and 9.9 MeV, but this energy region cannot be of importance to helium burning. His table of gamma ray angular distribution functions for this reaction were useful, however.

The J=2 level at 4.969 MeV in ^{20}Ne is extremely important, and would dominate the astrophysical rates if it could be formed from an α particle and ^{16}O. Gove, Litherland, and Clark (1961), however, have determined its parity to be negative, eliminating it from further consideration. The spins and parities of the levels at 5.63 and 5.80 MeV excitation have been measured by Kuehner (1961).

II. EXPERIMENTAL APPARATUS

A. Beam Source and Target System

The α-particle and proton beams for this experiment were obtained from the Kellogg Radiation Laboratory 3 MV electrostatic generator. The beams were analyzed by a 90° double-focussing magnet, and the generator's terminal voltage was regulated by signals from a pair of slits, placed after the magnet, that intercepted a fraction of the beam. The regulating slits and the remainder of the system are drawn schematically in Figure 3. The vacuum in the accelerating column and in the beam tube was obtained with oil diffusion pumps provided with refrigerated baffles.

After passing the slits, the beam entered a 38 cm. long, liquid nitrogen filled trap, which was the first section of a "clean" system, designed to eliminate hydrocarbon vapors from the target chamber, therefore reducing the buildup of carbon on the target. Carbon contamination created background in gamma spectrum through the detection of neutrons from the $^{13}C(\alpha,n)^{16}O$ reaction.

Continuing downstream, the beam passed an 8 liter/second ion pump, then entered the final slit assembly and target chamber. In addition to the ion pump, a molecular sieve, liquid-nitrogen-cooled sorption pump was used to rough the system from atmospheric pressure to a vacuum at which the ion pump

FIGURE 3: Experimental Apparatus

This is a schematic diagram of the experimental apparatus. The items designated 1, 2, and 3 are the target, electron suppressor, and beam defining aperture, respectively. The electron suppressor was maintained at -300 volts. (The diagram is not drawn to scale.)

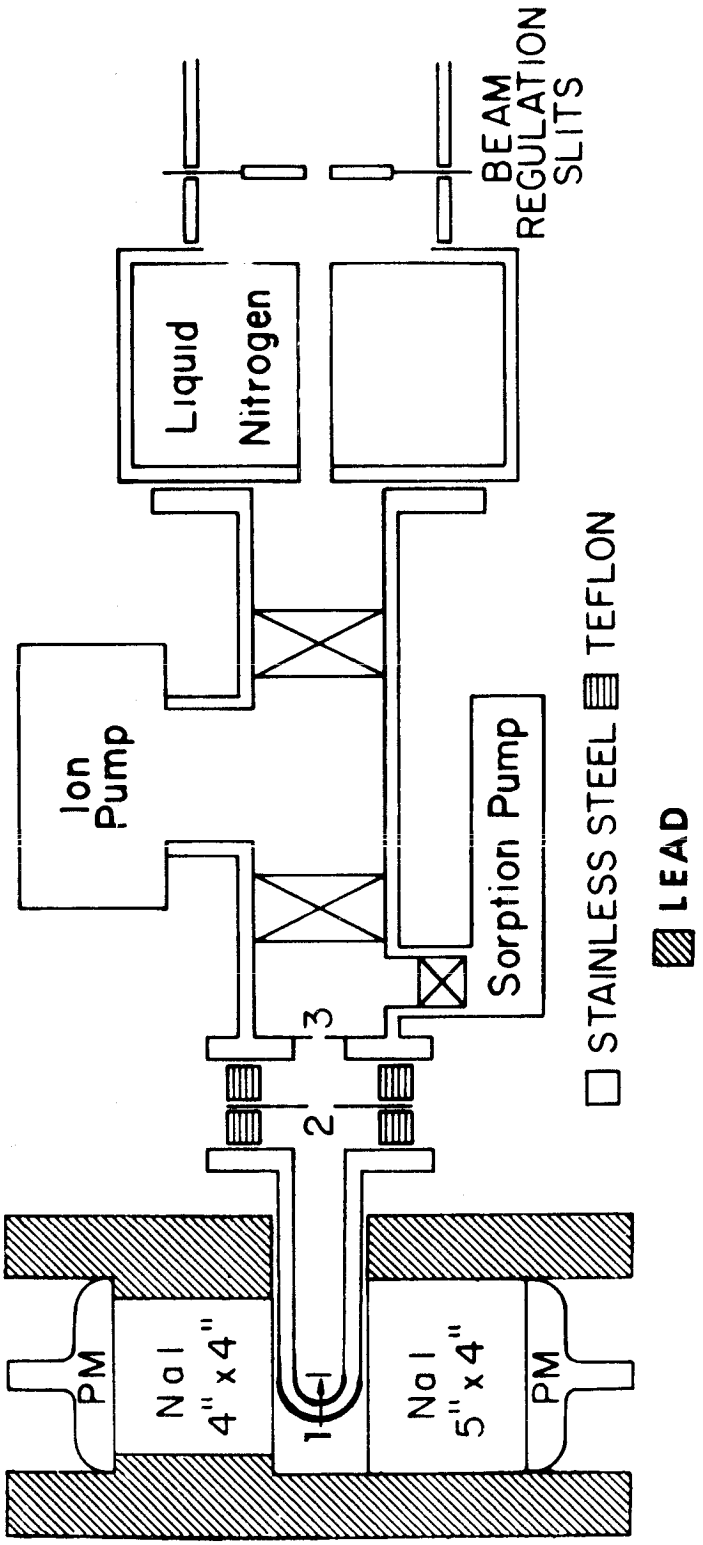
BEAM REGULATION SLITS
Liquid Nitrogen
Ion Pump
Sorption Pump
STAINLESS STEEL
TEFLON
LEAD
PM
NaI 4" x 4"
NaI 5" x 4"
PM
1
2
3

could operate efficiently. Thus, there was no hydrocarbon pumping whatsoever in the clean system.

The slit assembly consisted of a tantalum collimator that defined the diameter of the beam pencil to be 3/16 inch, followed by an electrically insulated suppressor, which was slightly larger than the collimator, and coaxial with it. The suppressor was maintained at a potential of -300 volts with a battery, to ensure accurate beam current integration by keeping electrons from upstream slits out of the target chamber, and keeping secondary target electrons inside the chamber.

The target chamber itself was fabricated from tubular stainless steel in a tee configuration, and arranged so that the beam entered the base of the tee. The targets were mounted on a water cooled copper block that entered one arm of the tee, and made electrical contact with it, so that the entire chamber acted as a Faraday cup. A viewing port on the other arm facilitated alignment of the target chamber and the gamma spectrometer with respect to the beam axis.

O-ring seals were used sparingly throughout the clean system, and, where they were necessary, viton o-rings were used. Low vapor pressure grease was used only on the sliding seal between the target mounting block and the chamber.

B. The Gamma Spectrometer

The properties of various scintillators are discussed in

detail by Neiler and Bell (1965) and Harshaw (1962). One very desirable property of thallium-activated sodium iodide for gamma detection is the relatively high charge of the iodine nucleus (Z=53). The three primary processes by which gamma rays interact with matter are the photoelectric, Compton, and pair processes, for which the dependence of the interaction cross section on the Z of the material is $Z^{\approx 5}$, Z, and Z^2, respectively. NaI will clearly be a much more efficient detector than organic scintillators (for carbon, Z=6), and although other phosphors such as CsI and KI have a slightly higher average Z, the shorter decay constant and higher light output of NaI(Tl) make it the better choice for present purposes.

Lithium-drifted germanium solid state counters possess resolution that is far superior to the resolution of a NaI(Tl)-phototube system, but the low efficiency (Z=32) and small size of the available Ge(Li) counters rules out their application here. The resolution of the NaI system, although not excellent, is usable, and with large crystals, high efficiency can be obtained, so sodium iodide was chosen for the detection system.

Two NaI(Tl) crystals, obtained from the Harshaw Chemical Company, were placed on opposite sides of the target, as shown in Figure 3. The distance from the center of the beam spot to the face of each crystal container was 3/4 cm. The larger crystal was 12.7 cm. in diameter and 10.2 cm. long, and was

viewed by a CBS 7819 photomultiplier tube, and the other crystal, 10.7 cm. diameter by 10.7 cm. long, was viewed by an RCA 2065 phototube. The two photomultiplier tubes were selected by the Harshaw Company for exceptional gain stability under changing count rates. As can be seen in Figure 3, the crystals were shielded with three to four inches of lead, which reduced the background from cosmic rays, natural radioactivity, and X-rays from the accelerator's high voltage terminal.

The electronic system is pictured in Figure 4. Each phototube was powered by a typical high-voltage dividing circuit and DC supply. The phototube gains were matched by varying the high voltage supplies. The dividing circuits were each followed immediately by a charge sensitive preamplifier, and the preamplifier outputs were fed into both an auxiliary coincidence circuit, to be described later, and a common summing network, which passively summed the two preamp outputs, so that the two crystals acted effectively as one large crystal in this circuit. Hereafter, this circuit will be referred to as the "sum mode circuit." The summed signal was amplified, and then fed into both a 400 channel pulse height analyzer (PHA), and a single channel analyzer (SCA). The latter was set to monitor the peak counts from gamma rays to the ground and first excited states (γ_0 and γ_1 transitions) of the product nucleus for the reaction of interest.

FIGURE 4: Electronics

The electronic pulse-handling networks are shown in block diagram. The following abbreviations are used: HV-adjustable D.C. high voltage supply, AMP-amplifier, SCA-single channel analyzer, PHA-pulse height analyzer, BCI-beam current integrator, and COIN-coincidence gate. The numbered arrows lead to the corresponding inputs of the two coincidence gates.

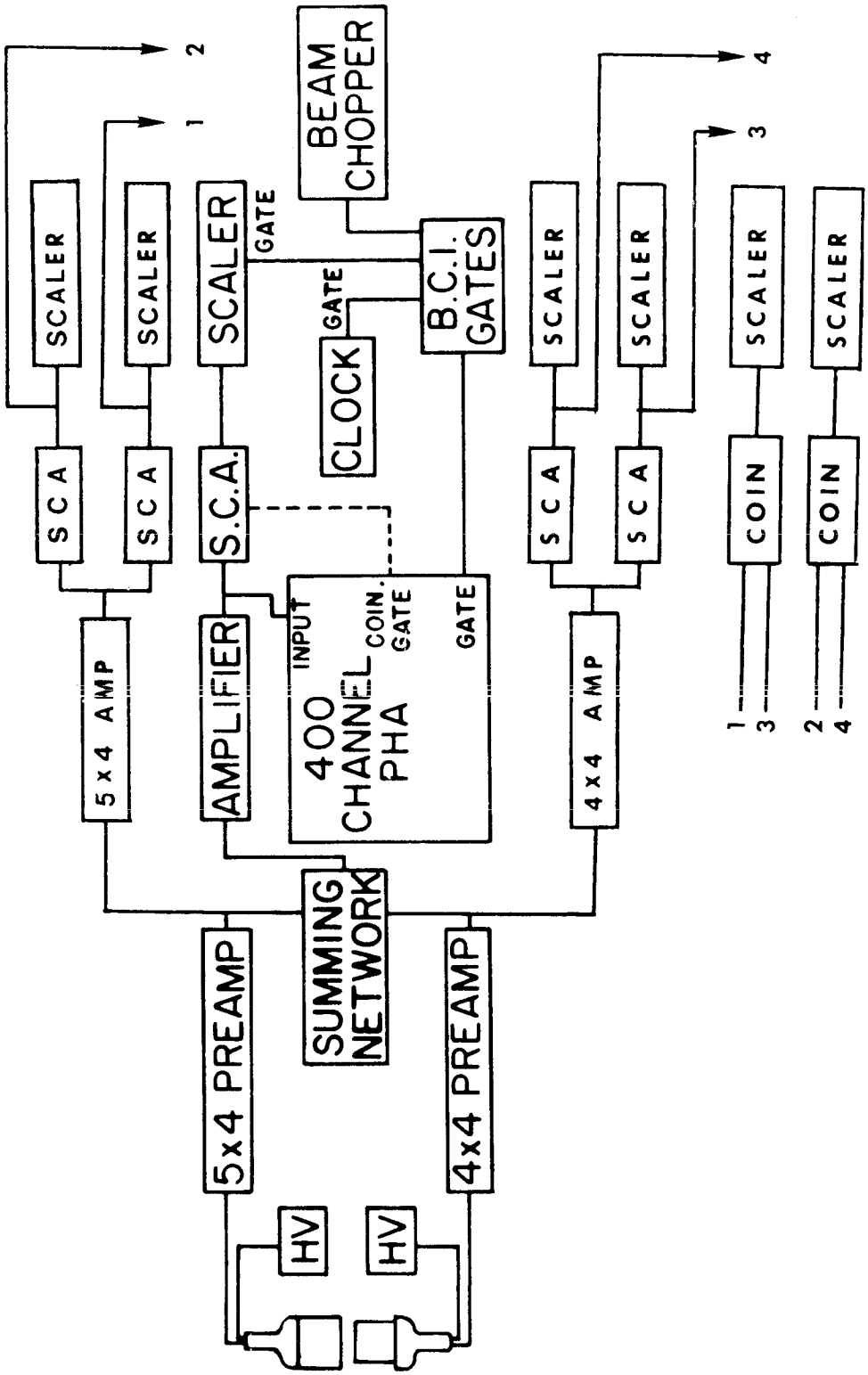
BEAM CHOPPER
SCALER
SCALER
SCALER
GATE
B.C.I. GATES
CLOCK
GATE
SCALER
SCALER
SCALER
SCALER
1
2
3
4
SCA
SCA
S.C.A.
SCA
SCA
COIN
COIN
5x4 AMP
AMPLIFIER
INPUT
400 CHANNEL PHA
COIN. GATE
GATE
4x4 AMP
1
3
2
4
SUMMING NETWORK
5x4 PREAMP
4x4 PREAMP
HV
HV

As mentioned above, each preamp also fed an auxiliary circuit, consisting of an amplifier followed by several single channel analyzers for each detector, followed by a pair of coincidence gates. By setting the SCA windows appropriately, the coincidence system could be set to require simultaneous detection of both members of a double cascade. This proved to be a valuable aid in identifying the reaction responsible for an observed resonance.

The SCA windows were set by using their outputs to gate the pulse height analyzer (indicated by dotted line in Figure 4), and observing the admitted spectrum in the pulse height analyzer. Each SCA and each coincidence gate was monitored by a scaler. A clock kept track of the real time, and the 400 channel analyzer was equipped with an internal clock that registered the total live time of the analog-to-digital converter. A beam current integrator gated the scalers, the 400 channel analyzer, and a magnetic beam chopper. The integrator was calibrated at least once daily.

III. DETECTION EFFICIENCY FOR SINGLE GAMMA RAYS

A. Calibration of the Original Spectrometer

The spectrometer efficiency for detecting single, or monochromatic, gamma rays of various energies must be known before the detection efficiency for a complex cascade can be discussed. As mentioned in the introduction, the spectrometer used in the present investigation is a slightly modified version of the original spectrometer. The experimental calibration of the single gamma efficiency of the original spectrometer was described in PBL and LTS, and will be outlined here. The effect of the modifications on the detection efficiency was calculated to be small, and this was checked experimentally at the most important energy.

For the geometry used in these measurements, the detection efficiency, $\epsilon(E)$, where E is the gamma energy, will be defined as the probability that a gamma ray, emitted from a source located centrally between the two crystals, will cause a pulse to be registered somewhere in the spectrum. In principle, $\epsilon(E)$ could be calculated for any geometry with the help of gamma ray attenuation coefficients, such as those given by Grodstein (1957). For totally bare NaI crystals, this would be a feasible approach, and $\epsilon(E)$ could be calculated from the following formula

$$\epsilon(E) = \frac{1}{2}\int_{NaI}\left\{1 - \exp\left[-\mu(E,NaI)X(\theta)\right]\right\}\sin\theta\, d\theta \qquad (7)$$

where $\mu(E,NaI)$ is the attenuation coefficient at energy E for NaI (from Grodstein, 1957), $X(\theta)$ is the path length in NaI at angle θ, measured from the crystal axis, and the axial symmetry eliminates the integration over ϕ. This formula neglects the effects of anisotropy in the gamma ray angular distribution, which are mostly averaged out by the large solid angle ($\approx$80% of 4π) subtended by the crystals. Although minor, the effects will be discussed in a later section. The present discussion assumes that the gamma decays are isotropic.

In the actual system, various objects, between the source and the NaI, could interact with γ rays from the source, and therefore influence the detection efficiency. These objects include the target backing, target chamber walls, crystal containers, and the reflecting material surrounding the crystals. All such material will be referred to as absorber.

The absorber effects are hard to calculate for several reasons. The scattered γ rays from Compton events in an absorber may or may not interact with the NaI. The fates of energetic electrons from other gamma interactions in an absorber are similarly uncertain. For these corrections, one can only make "best estimates," although two limiting cases can be calculated readily, and provide rough upper and lower bounds for the efficiency. The lower limit is obtained by assuming that all absorber events are lost; that is, no electron or Compton gamma interacts with the NaI. For this case, the efficiency is given by

$$\epsilon(E) = \frac{1}{4\pi}\iint_{NaI} \exp\left[-\sum_i \mu_i(E,\text{abs.})X_i(\theta,\phi)\right]\left\{1 - \exp\left[-\mu(E,NaI)X(\theta)\right]\right\} \sin\theta\, d\theta d\phi \qquad (8)$$

where the sum is over the path length-attenuation coefficient products for the various absorbers. All attenuation coefficients were taken from Grodstein (1957).

The upper limit to the efficiency is calculated by assuming that all absorber events, in the cones subtended by the NaI, result in interactions in the NaI, and is given by

$$\epsilon(E) = \frac{1}{4\pi}\iint_{NaI}\left\{1 - \exp\left[-\sum_i \mu_i(E,\text{abs.})X_i(\theta,\phi) - \mu(E,NaI)X(\theta)\right]\right\}\sin\theta\, d\theta d\phi \qquad (9)$$

The calculated efficiencies for the three cases are shown in Figure 5. The dashed, lower dotted, and upper dotted curves were calculated with Equations 7, 8, and 9, respectively. Uncertainties in the calculations arise from several sources. Grodstein estimates an uncertainty of 5% for the attenuation coefficients. An error of 1 mm. in the measured distance from the source to the front of the NaI container, would change the efficiency by about 3 and 3.6 % for the 5" x 4" and 4" x 4" crystals, respectively. An error of about 1 mm. could have arisen from X-ray measurements of the thickness of the MgO reflector, packed between the NaI crystal and the aluminum container. The photonuclear cross sections for sodium and iodine are small, and can be neglected.

FIGURE 5: Detection Efficiency (Original Geometry)

Both calculated and experimentally determined detection efficiencies are shown in the figure--all for the original spectrometer geometry. The two dotted curves and the dashed curve were calculated for the special cases described in the text, using Equations 7, 8, and 9. The experimental calibration data are represented by the numbered points. The solid curve represents the efficiencies used with the original geometry. The numbered points were determined with:

1) ^{54}Mn and ^{88}Y sources
2) The $^{23}Na(p,\alpha_1\gamma)^{20}Ne$ reaction
3) ^{88}Y source
4) The $^{15}N(p,\alpha_1\gamma)^{12}C$ reaction
5) The $^{29}Si(p,\gamma)^{30}P(\beta^+)^{30}Si$ reaction
6) The $^{19}F(p,\alpha_1\gamma)^{16}O$ reaction
7) The $^{27}Al(p,\gamma)^{28}Si$ reaction
8) The $^{27}Al(p,\gamma)^{28}Si$ reaction
9) The $^{11}B(p,\gamma)^{12}C$ reaction

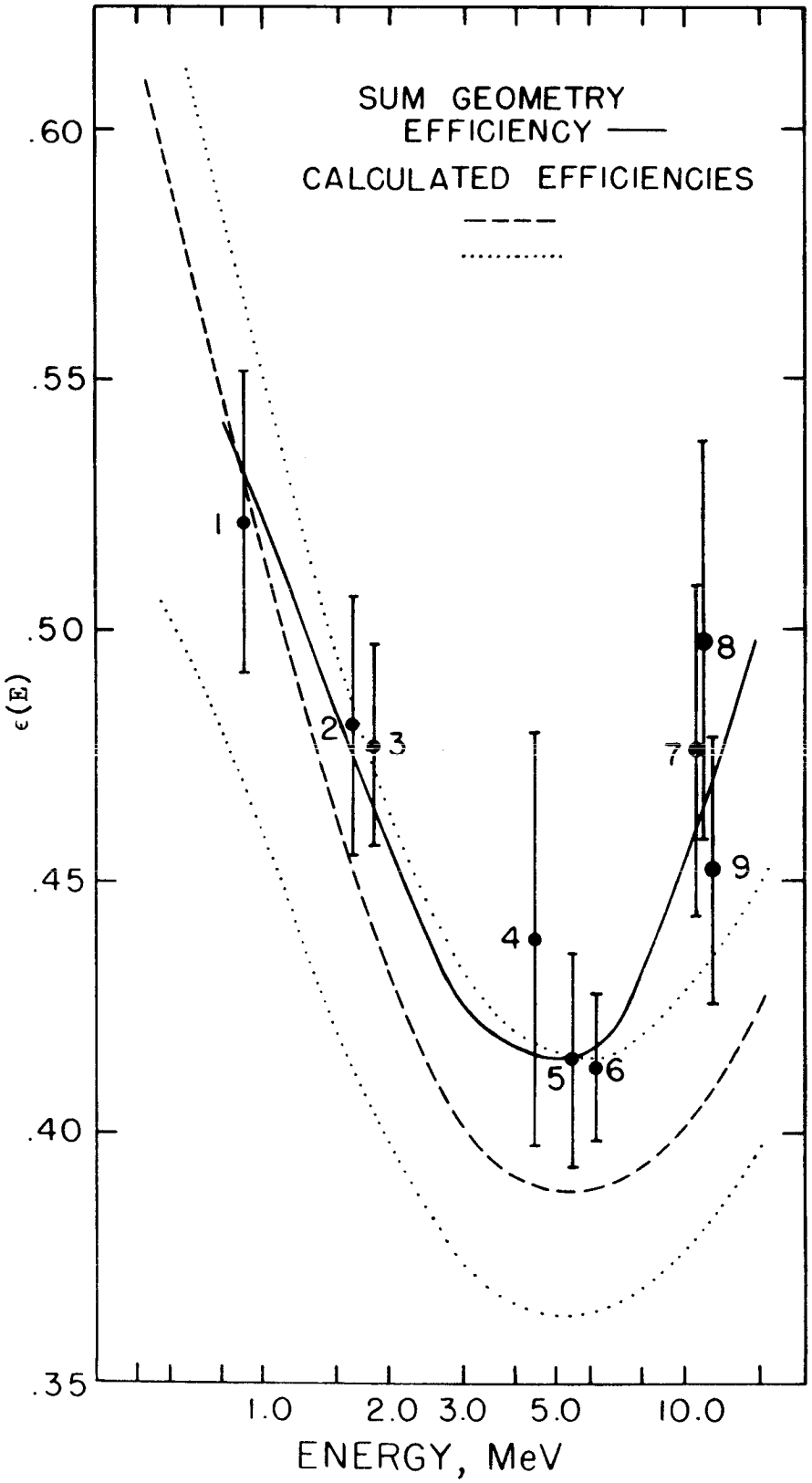
SUM GEOMETRY
EFFICIENCY ——
CALCULATED EFFICIENCIES

.....
.60
.55
.50
.45
.40
.35
ε(E)
1
2
3
4
5
6
7
8
9
1.0
2.0
3.0
5.0
10.0
ENERGY, MeV

Also appearing in Figure 5 are the experimental data, and the solid curve through the data points represents the efficiencies adopted for the unmodified spectrometer. In view of the errors just discussed, the deviation of the solid curve from the envelope defined by the two dotted curves (which represent limiting cases) is not considered to be serious. The experimental points were determined in the following several ways.

a) Points 1 and 3 in Figure 5 were obtained with ^{88}Y and ^{54}Mn radioactive sources. Weak sources (≈0.1 uCurie) were prepared by evaporating small quantities of radioactive solutions on a standard target backing, and then calibrating the fabricated sources with standard sources obtained from the Radiochemical Centre, England, and the Commissariat à l'Energie Atomique, France. The standard deviations quoted for these sources were 2%. The radioactive solutions were obtained from the General Radioisotopes Processing Corporation (San Ramon, California). The ^{54}Mn source yielded the detection efficiency for a 0.835 MeV γ ray. Since the ^{88}Y spectrum contains both 0.90 and 1.84 MeV γ rays, the shape from the ^{54}Mn spectrum was used to remove the contribution in the ^{88}Y spectrum from the 0.90 MeV gamma. This procedure yielded the efficiencies at E_γ = 0.90 and 1.84 MeV (points 1 and 3).

b) Several $(p,\alpha_1\gamma)$ reactions were used to obtain the data points 2, 4, and 6. For these measurements, an Ortec

surface barrier detector, mounted behind a circular aperture on one leg of the target chamber, monitored the α particles, while the gammas were counted by the spectrometer in the usual way. Coincidence between α particles and γ rays was not required, but the beam current integrator gated both counting systems simultaneously. Since the area of the aperture and the distance between the aperture and the source could be measured quite accurately, the detection efficiency for the α particle system was well known. The gamma detection efficiency was therefore obtained by direct comparison of the number of counts in the alpha and gamma spectra. Angular distributions were taken from the literature to correct for anisotropy in the distribution of the α particles. Points 2, 4, and 6, at 1.63, 4.43, and 6.13 MeV, were obtained with the reactions $^{23}Na(p,\alpha_1\gamma)^{20}Ne$, at E_p=1163 keV, $^{15}N(p,\alpha_1\gamma)^{12}C$, at E_p=898 keV, and $^{19}F(p,\alpha_1\gamma)^{16}O$, at E_p=341 keV, respectively.

c) Point 5, at 5.3 MeV, was obtained from the reaction, $^{29}Si(p,\gamma)^{30}P(\beta^+)^{30}Si$. A 4π β counter was constructed from two cylinders of Pilot B plastic scintillator, and used to count the positrons from the ^{30}P decay. The target was bombarded by 416 keV protons, then quickly transferred to the 4π β counter. The transfer took typically one minute, reasonably short compared with the ^{30}P half-life of 2.5 minutes. The gamma rays were counted as usual during the proton bombardment. A system constructed by Dr. Dale Hebbard and Mr. Harold Spinka accurately

monitored the beam current as a function of time, and kept track of the sequential counting periods. This information, along with the positron spectrum, provided a direct determination of the gamma detection efficiency at 5.3 MeV.

d) The $^{27}Al(p,\gamma)^{28}Si$ reaction, at E_p=992 and 1388 keV, provided points 7 and 8, at 10.76 and 11.14 MeV. The $^{11}B(p,\gamma)^{12}C$ reaction, at E_p=163 keV, provided point 9, at 11.7 MeV. For each of these resonances, it was known from the literature that the decay of the excited level was dominated by a transition through the first excited state of the product nucleus. Since the detection efficiency for the low energy member of the cascade was already known from the work just described, the detection efficiency for the high energy member was readily obtained.

B. Detection Efficiency for the Modified Spectrometer

Two changes were made in the original spectrometer, prompting careful thought about their effect on the detection efficiency. The first change involved the addition of about 1000 pounds of lead shielding to the original spectrometer, which had no shielding. The lead is pictured in Figure 3.

The detection efficiency would be enhanced if an interaction between a primary gamma (from the target) and the lead were to scatter an electron or secondary gamma ray into the NaI. The geometry of the system, however, requires that, in order to enter the NaI, the secondary particle must be emitted at a

back angle ($>90^{\circ}$) with respect to the primary gamma, or else be scattered at least twice. The back angle restriction severely limits the energy that can be deposited in the NaI, as can be seen by considering the fundamental interaction processes.

a) For the photoelectric effect, the photoelectron must scatter into the forward cone

b) For pair production, the positron and electron go predominantly into the forward cone, and, since the quanta from the subsequent positron annihilation must be emitted in opposite directions, this process can at most contribute a single 0.511 MeV quantum to the detector

c) For Compton scattering, the electron again must scatter into the forward cone, and, from the well-known Compton formula,

$$\Delta\lambda = \frac{h}{m_e c}(1 - \cos\theta),$$

it is evident that, for $\theta > 90^{\circ}$, the wave length of the scattered gamma will be greater than the electron's Compton wave length, and therefore, the gamma energy will be less than 0.511 MeV, the electron's rest mass.

Since, in analysis, the gamma spectra have always been extrapolated horizontally to zero for pulse heights below about 1 MeV (PBL), counts at 0.5 MeV or less would not affect the final result, and their contribution to the spectrometer efficiency can therefore be neglected.

The effects of multiple scattering events are harder to estimate, but as such events should be relatively rare, their contribution should not be important.

The validity of the above arguments was tested with an experimental check. Spectra were taken of the 6.13 MeV gamma ray from $^{19}F(p,\alpha_1\gamma)^{16}O$, both with and without the lead. The detection efficiency changed less than 1%, so the effects of the shielding were neglected.

The second modification involved the introduction of a stainless steel target chamber, which replaced the earlier pyrex chamber. This had two effects on the detection efficiency. First, the wall thickness, in mg/cm^2, of the steel chamber was substantially greater than that of the pyrex chamber, resulting in about 2% greater attenuation of primary gammas at 1-3 MeV. Between 3 and 7 MeV, the thicker wall stopped some of the electrons that had originated in primary interactions in the target backing (these account for about 6% of the total efficiency at 5 MeV), and, at higher energies, energetic electrons produced from interactions in the chamber walls contributed to the efficiency.

The second effect of the chamber was simply due to the slightly larger size of the steel chamber, which required greater distance between the target and the crystals; this decreased the subtended solid angle, and therefore the efficiency, by $(3\pm1)\%$.

These corrections were included in a "best" calculation for the detection efficiency for the modified system, which included absorber effects. The final efficiency curve adopted for the modified system was then obtained in the following way. A similar "best" calculation had been made for the original geometry; the ratio of the experimental efficiency to this calculated efficiency was used to correct the "best" calculation for the modified system. This procedure can be expressed in the following way:

$$\epsilon(E_\gamma) = \epsilon(E_\gamma, \text{ calc., modified}) \frac{\epsilon(E_\gamma, \text{ exper., original})}{\epsilon(E_\gamma, \text{ calc., original})} \qquad (10)$$

where calc.= calculated and exper.= experimental. Figure 6 illustrates the experimental curve for the original geometry (curve 1), the best calculation for the modified geometry (curve 2), and the efficiency, calculated with Equation 10, used for the modified system (curve 3). Since the two "best" calculations were based on similar assumptions, it was believed that this procedure would tend to eliminate similar errors in the calculations. The uncertainty in the efficiency is estimated to be not worse than 6% for γ rays less energetic than 8 MeV, and 10-12% for higher energies. As a check, the efficiency was measured in the modified geometry at 6.13, using again the $^{19}F(p,\alpha_1\gamma)^{16}O$ reaction; the result is indicated by the triangular point in Figure 6. The original experimental points were included

FIGURE 6: Detection Efficiency (Modified Geometry)

This figure illustrates the experimentally determined efficiency for the original geometry (curve 1), the best calculation for the modified geometry (curve 2), and the efficiency, calculated with Equation 10, for the modified system. The triangular datum is the experimental result for the modified system, and the circular data are the experimental results for the original system (as in Figure 5).

Curve 3 is the efficiency curve adopted for the modified geometry.

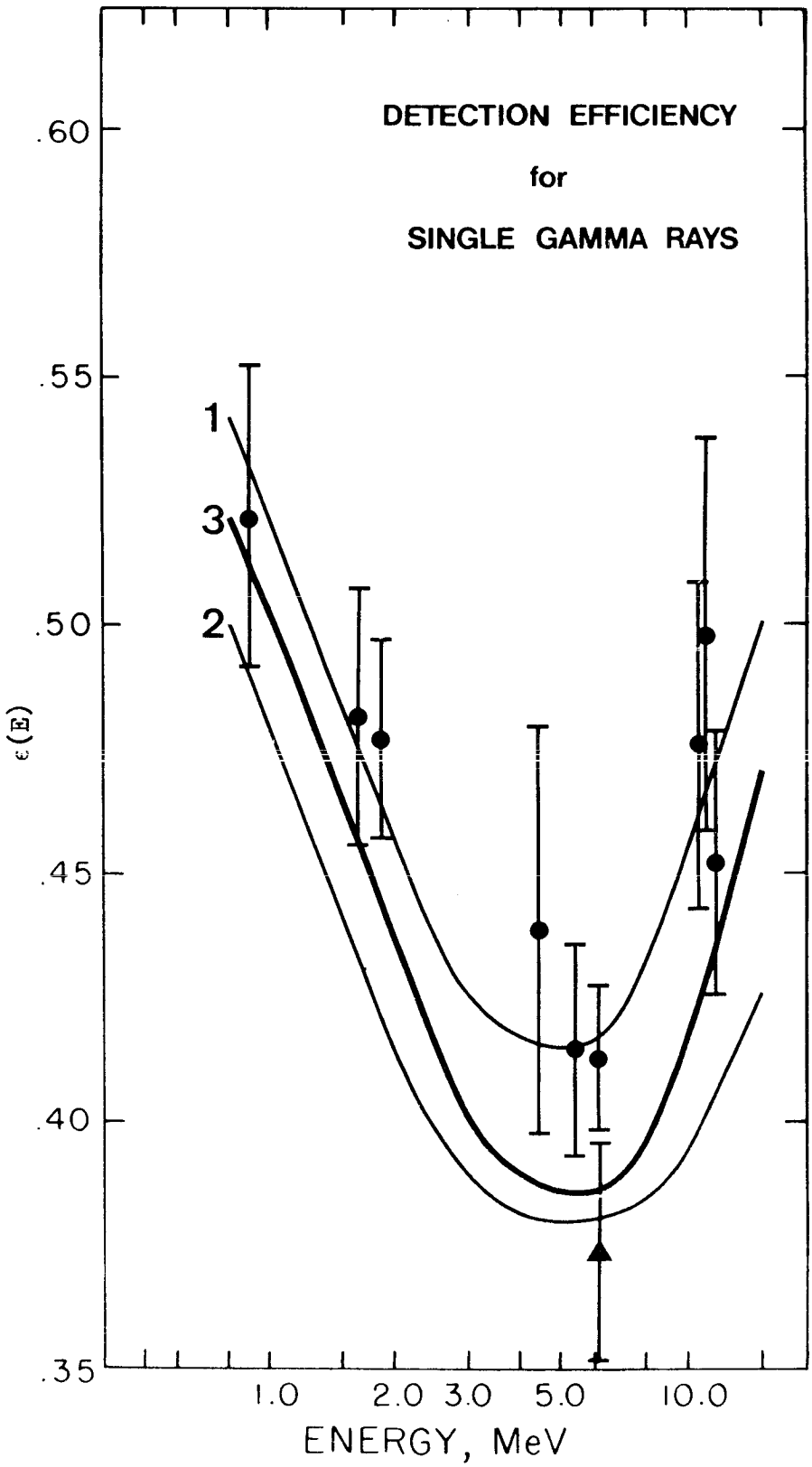
DETECTION EFFICIENCY
for
SINGLE GAMMA RAYS
.60
.55
.50
.45
.40
.35
ε(E)
1
3
2
1.0
2.0
3.0
5.0
10.0
ENERGY, MeV

to illustrate that the change in the efficiency for the modified system is roughly equal to the magnitude of the standard deviations of the experimental data.

C. Angular Distribution Corrections

As mentioned before, the effects due to anisotropy of the gamma decay should be weakened, because the large detectors integrate over a major fraction of the solid angle. However, a quantitative examination of this statement would seem prudent.

In the previous section, isotropy was assumed for the gamma decay. In general, the decay is not isotropic, and the angular distribution can be expressed as

$$W(\theta') = \sum_L a_L P_L(\cos \theta') \qquad (11)$$

where θ' is measured with respect to the beam axis (θ still refers to the coordinate system whose z axis is the symmetry axis of the cylindrical crystals), the P_L are the Legendre polynomials, $a_0 = 1$, and, because of symmetry, $a_L = 0$ for all odd L. Then the number, $N(\theta')$, of gammas emitted into $d\Omega$ at angle θ', is

$$N(\theta') = \frac{N_\gamma}{4\pi} W(\theta')d\Omega, \qquad (12)$$

for a monochromatic gamma ray. The efficiency, which was defined as the ratio of the number of detected γ rays to the number emitted, is given by

$$\epsilon = \frac{1}{4\pi}\iint W(\theta' = \theta + \beta)\left\{1 - \exp\left[-\mu(\mathrm{NaI})X(\theta)\right]\right\} d\Omega \qquad (13)$$

where β is the angle between the beam axis and the crystal axis ($\beta = 90^{\circ}$ for this spectrometer). The only difficulty in performing the integral involves expressing the individual P_L's in terms of the unprimed θ coordinate. From the study of rotations, it is well known that the spherical harmonics transform as follows

$$Y_L^{M'}(\Omega') = \sum_M D^L_{MM'}(\alpha\beta\gamma)\, Y_L^M(\Omega) \qquad (14)$$

where the $D^L_{MM'}$ are the rotation matrices, and α, β, and γ are the usual Euler angles. The notation of Rose (1957) will be used throughout the discussion. The $D^L_{MM'}$ can be broken down into

$$D^L_{MM'} = e^{-iM\alpha} d^L_{MM'}(\beta) e^{-iM'\gamma} \qquad (15)$$

Since there need be no rotation about the z axis for the present problem, γ may be chosen as zero. Furthermore, the desired transformation is for $P_L(\cos\theta')$ which may be expressed as

$$P_L(\cos\theta') = \sqrt{\frac{4\pi}{2L+1}}\, Y_L^0(\theta', 0). \qquad (16)$$

Therefore, $M' = 0$. Noting that, for the special case of axially symmetric detectors, the only ϕ dependence resides in the $\exp(iM\phi)$ dependence of the spherical harmonics, so that the integration over ϕ will remove all but the $M = 0$

term, only $d^{L}_{00}(\beta)$ is required, which is just $P_L(\cos\beta)$. The efficiency integral becomes

$$\epsilon = \frac{1}{2}\sum_L a_L P_L(\cos\beta)\int P_L(\cos\theta)\left\{1-\exp[-uX(\theta)]\right\}\sin\theta\, d\theta. \quad (17)$$

If the integral is replaced by $\epsilon_{iso}Q_L$, where ϵ_{iso} is the efficiency for isotropic decay, thus defining Q_L (Rose's smoothing factors), then the ratio of anisotropic to isotropic decay efficiencies is

$$\frac{\epsilon}{\epsilon_{iso}} = \sum_L a_L P_L(0) Q_L, \quad (18)$$

where the value $\beta=\pi/2$ has been inserted for the spectrometer used in this work.

The Q_L have been calculated for this spectrometer, neglecting absorber effects because they represent a second-order correction and introduce a further φ dependence, rendering the integral in Equation 13 more difficult. The results (PBL, LTS) are, for the 4" x 4" crystal, $Q_2 = 0.29$ and $Q_4 = -0.060$; and for the 5" x 4" crystal, $Q_2 = 0.25$, and $Q_4 = -0.075$. For higher L values, the Q_L's are negligible.

As mentioned, this discussion assumed the emission of a single gamma. For multiple cascades, involving angular correlations, the calculation would involve the Q_L's to powers of 2 and greater (Rose, 1953), which can be neglected for this geometry.

For the levels studied in $^{16}O(\alpha,\gamma)^{20}Ne$, the multipolarity

of the radiation was known, and the small efficiency corrections were included in the calculations of the resonance strengths. For the $^{28}Si(\alpha,\gamma)^{32}S$ reaction, new levels were found for which the character of the radiation was neither known nor easily determined with this system. Assuming a worst case, the α particle could be captured in a p-wave, exciting a 1^- level. Since the 0^+ alpha and the 0^+ ^{28}Si nucleus could form only a $J_z = 0$ level, the multipole pattern is determined, and the angular distribution would have the form:

$$W(\theta') = 1 - P_2(\cos \theta'). \qquad (19)$$

This angular distribution would require a correction of about 13% to the isotropic efficiency. Since it is highly unlikely that the cascade structure would be this simple for levels that might be excited in this reaction, an uncertainty of just 10% has been included in the $^{28}Si(\alpha,\gamma)^{32}S$ yield analysis to cover angular distribution effects.

IV. DETERMINATION OF N_γ FOR A TYPICAL LEVEL

As illustrated in Section IC, the total number of times that the resonant level decayed by γ emission, N_γ, must be determined from the resonance spectrum and knowledge of the spectrometer efficiency. Note that N_γ is not, in general, equal to the number of γ rays emitted from the target. Equality would hold only for the special case in which the level decayed only by a direct ground state transition (γ_0); otherwise, N_γ is smaller than the number of γ rays emitted. A relationship between N_γ, the spectrometer efficiency, and the number of counts registered in some portion of the spectrum, must be determined in order that the resonance strength may be calculated. A different method was used for each of the reactions studied here.

A. Determination for $^{16}O(\alpha,\gamma)^{20}Ne$

If the experimental situation provides a spectrum that is usable to a low enough energy that an extrapolation to zero energy will provide a reasonably accurate representation of the shape, the total number of detected events, or counts, N_C, can be obtained simply by integrating over the entire spectrum. By defining ϵ_T as the total probability that the decay of the level by gamma emission will be recorded by a count in the spectrum, the yield may be represented by

$$N_\gamma = \epsilon_T N_C , \tag{20}$$

where ϵ_T will depend on the cascade structure of the resonance. If the cascade structure is well understood, ϵ_T can be calculated as follows, using the single gamma detection efficiencies, $\epsilon(E)$, discussed in the preceding section. For a level that decays only through one intermediate state, emitting two γ rays of energy E_1 and E_2, the probability that neither gamma interacts, $(1 - \epsilon_T)$, is clearly just $(1 - \epsilon(E_1))(1 - \epsilon(E_2))$, yielding

$$\epsilon_T = 1 - (1 - \epsilon(E_1))(1 - \epsilon(E_2)) \tag{21}$$

For a complex cascade, involving several different transitions, this can be generalized to

$$\epsilon_T = \sum_i \beta_i \left(1 - \prod_j [1 - \epsilon(E_{ij})]\right) \tag{22}$$

where β_i is the i^{th} branching ratio, or the fractional probability that the level decays through the i^{th} cascade; E_{ij} is the energy of the j^{th} member of the i^{th} cascade; and the product is taken over all members of the i^{th} cascade.

For the $^{16}O(\alpha,\gamma)^{20}Ne$ reaction, the branching ratios were available in the literature (Van der Leun et al., 1965), and the resonance spectra were clean enough that N_C could be calculated.

B. Determination of N_γ for $^{28}Si(\alpha,\gamma)^{32}S$

For this reaction, information concerning the cascade structure was not available in the literature for the previously studied resonance, and clearly not available for any of the new resonances. In addition, background counts, due primarily to the $^{13}C(\alpha,n)^{16}O$ reaction, rendered the spectra useless at low energies, and therefore, N_C could not be extracted. A similar situation, encountered by PBL and LTS in their study of $^{27}Al(p,\gamma)^{28}Si$, prompted an investigation of the influence of cascade structure on the probability that the system would detect the decay of the resonance level by registering a count in a specified portion of the spectrum; that portion being anywhere above a bias energy, E_B. For 22 resonances in $^{27}Al(p,\gamma)^{28}Si$, for which the branching ratios were known and N_C could be extracted, the dependence of the detection probability just defined on E_B was studied. The probability, called the partial detection efficiency, $\eta(f)$, was calculated from

$$\eta(f) = \frac{N_B(f)}{N_C} \epsilon_T , \qquad (23)$$

in which:

ϵ_T is the resonance efficiency defined in Equation 22

f is the bias fraction, E_B/E_X, where E_X is the excitation energy of the resonance level

$N_B(f)$ is the integral of the spectrum from E_B to infinity.

Clearly, for f=0, $N_B(0)=N_C$, and $\eta(0)=\epsilon_T$. A catalog of "η curves" was constructed, using spectra obtained for the 22 resonances in the original detector geometry, and the main features are shown in Figure 7. The dotted and dashed curves represent averages for resonances whose decays are dominated by ground state (γ_0), first excited state (γ_1), and multiple (2γ, 3γ, etc.) transitions, and their qualitative features are what one would expect. The solid curves represent the extreme value of $\eta(f)$, at each value of f, for all 22 cases. Since the resonances contained in the catalog covered a very wide variety of cascade types, the extreme curves should be reasonably good limits.

The interesting result from this study is that, for an f value of about 0.35, the extreme curves deviate by less than 13% from the median value, $\eta(0.35) = 0.37$. Therefore, for any level in ^{28}Si in this region of excitation (10-14 MeV), one may determine N_γ in the original geometry by

$$N_\gamma = \frac{N_B(f=0.35)}{(0.37 \pm 15\%)} \qquad (24)$$

The existence of this method for determing N_γ fulfills the requirement, expressed in Section IB, that the spectrometer efficiency be independent of cascade structure. The 15% error introduced by this assumption is acceptable in view of other uncertainties in the experimental procedure, and of the present state of astrophysical calculations.

FIGURE 7: Partial Detection Efficiencies for the Original Geometry

The dotted and dashed curves represent averages for resonances whose decays are dominated by the indicated transitions. The solid curves represent the extreme value, at each value of f, for all of the levels studied.

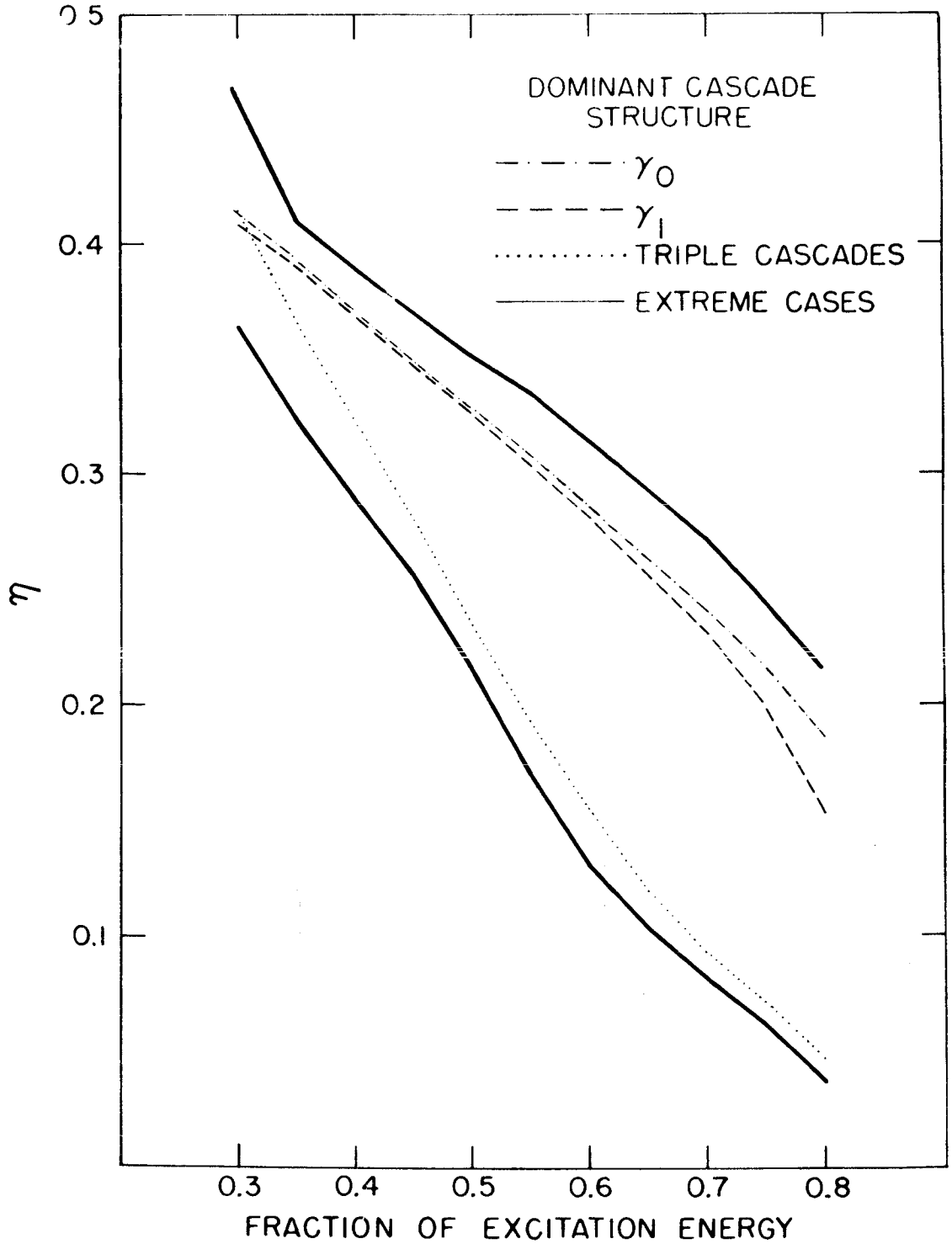
0.5
0.4
0.3
0.2
0.1
η
DOMINANT CASCADE STRUCTURE
γ_0
γ_1
TRIPLE CASCADES
EXTREME CASES
0.3
0.4
0.5
0.6
0.7
0.8
FRACTION OF EXCITATION ENERGY

Although the change in geometry should have had little effect on the shape of the partial detection efficiency curves, and a predictable change in their absolute value at f=0.35, it seemed prudent to remeasure several of the curves with the modified spectrometer. Three resonances in $^{27}Al(p,\gamma)^{28}Si$ were chosen; each one was strongly dominated by one of the three major types of cascades, and was therefore an extreme case and a good check. The resonance at a bombarding energy of 774 keV decays 72% of the time directly to the ground state, the resonance at 992 keV branches 76% by a γ_1 transition, and 96% of the decays of the 1118 keV resonance are 3γ or 4γ cascades. The branching ratios are listed in the review by Endt and Van der Leun (1967). The η curves measured with these resonances in the new geometry behaved as expected, and would suggest a new optimum value, $\eta(0.35) = 0.354$, which is 4.3% below the old value, and quite reasonable in view of the change in the single gamma efficiencies.

The η curves discussed so far were measured only for levels in the ^{28}Si nucleus, which raises a question regarding their applicability to levels in ^{32}S. As mentioned previously, η curves could not be obtained for the $^{28}Si(\alpha,\gamma)^{32}S$ resonances studied here, but the cascade structure has been determined for many levels in ^{32}S that can be excited with the $^{31}P(p,\gamma)^{32}S$ reaction. Although these levels are 0.5 - 1 MeV higher in excitation energy than the levels studied here with $^{28}Si(\alpha,\gamma)^{32}S$,

the range of excitation energies under study is 8.5 - 9.5 MeV, and the η curves would not be expected to vary appreciably in this region. The levels examined were at bombarding energies of 541, 642, 811, and 1438 keV, and their cascades were dominated by branchings of 80% γ_1, 77% γ_0, 57% γ_1, and 95% 3γ and 4γ, respectively (Endt and Van der Leun, 1967). The η curves measured for these resonances are shown in Figure 8. Although the optimum f for these four curves appears to be lower than 0.35, the spread at $f = 0.35$ is tolerable, and several of the spectra for resonances in $^{28}Si(\alpha,\gamma)^{32}S$ were not usable for enegies corresponding to $f < 0.35$. The mean value of the two extremes is $\eta(0.35) = 0.337$, which is 5% below the optimum value determined for ^{28}Si levels in the modified geometry, and well within the 15% uncertainty assigned earlier. Figure 8 indicates the optimum value for ^{32}S (circular datum with error bars), and the optimum value for ^{28}Si (triangular datum), both in the modified geometry.

Using this information, N_γ for the $^{28}Si(\alpha,\gamma)^{32}S$ resonances was calculated from

$$N_\gamma = \frac{N_B(0.35)}{(0.34 \pm 20\%)} \qquad (25)$$

where the 20% uncertainty includes both the error estimated in using the optimum η value, and the 10% uncertainty estimated for angular distribution effects, discussed in Section IIIC.

As a further check on the single gamma efficiency curve, the strength for the 992 keV resonance in $^{27}Al(p,\gamma)^{28}Si$ was determined, and compared with the value obtained by LTS, using the original geometry. The two values differed by 4%, which is within the 5% uncertainty assigned to each measurement for the determination of N_C(the total number of counts in the spectrum).

FIGURE 8: Partial Detection Efficiencies for the Modified System

The numbers on the four curves are the energies, in keV, of the resonances in $^{28}Si(\alpha,\gamma)^{32}S$ that the curves represent. The error bars on the ^{32}S optimum value are $\pm$ 20% of the value. This error includes both the uncertainty estimated to arise from the use of the optimum value, and the 10% uncertainty estimated for angular distribution effects, discussed in Section IIIC.

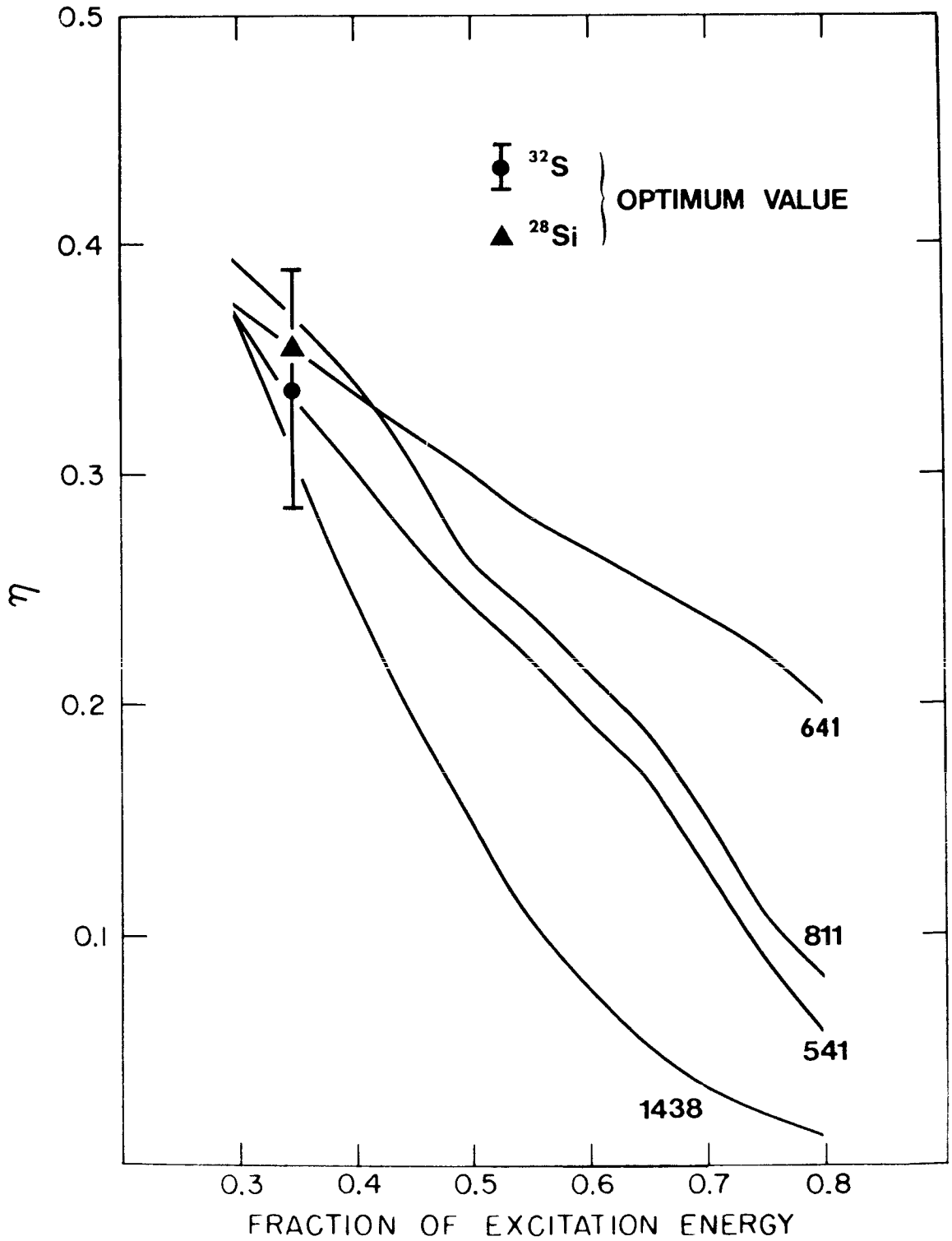
0.5
0.4
0.3
0.2
0.1
η
^{32}S
^{28}Si
OPTIMUM VALUE
641
811
541
1438
0.3
0.4
0.5
0.6
0.7
0.8
FRACTION OF EXCITATION ENERGY

V. THE $^{28}Si(\alpha,\gamma)^{32}S$ REACTION

A. Targets

The spectrometer described in the previous sections was used to investigate the $^{28}Si(\alpha,\gamma)^{32}S$ reaction for He^+ bombarding energies below 2.75 MeV. The first of the three targets used for this work was simply a rectangular piece of semiconductor grade silicon crystal. The beam continously deposited 10 - 20 watts in the front surface of the crystal, sufficient energy to cause the silicon to glow dull red. Examination of the crystal after bombardment showed obvious damage to the front surface; it was therefore felt that the possibility of channeling, which could have reduced the yield from the crystalline target, was eliminated. Because the target thickness was orders of magnitude greater than the range of 3 MeV α particles, the yield from this target was an integral of the reaction yield over all energies less than E_{He^+}. This target will be referred to as the stopping target.

The other two targets were made from elemental silicon, obtained from Oak Ridge National Laboratory, that had been enriched to 99.91% ^{28}Si, 0.06% ^{29}Si, and 0.03% ^{30}Si (the natural abundances are 92.21%, 4.70%, and 3.09%, respectively). A spectrographic analysis from the supplier provided upper limits to impurity concentrations, which were all less than 0.1% by weight. The important, low-Z contaminants, lithium,

beryllium, and boron, were present in concentrations of less than 0.005%, 0.001%, and 0.01% by weight, respectively.

Both targets were prepared in the following way: under vacuum, a layer of reagent grade copper, thick enough to stop 3 MeV α particles, was thermally evaporated onto a target blank of copper stock, 1 cm wide and 0.06 cm thick. While still under vacuum, a thin layer of silicon was evaporated onto the copper. The target was then removed from vacuum and screwed to a water cooled copper mounting piece. The assembly was then installed in the target chamber. The resulting targets were roughly 5 and 20 keV thick to 2 MeV alpha particles. They will be referred as the ^{28}Si thin targets (although the 20 keV target was thick enough for the yield to be calculated with Equation 4, Section IC).

Oxygen contamination in evaporated silicon targets is a common problem, arising probably because the silicon evaporates at such a high temperature that it will react readily with residual oxygen in the vacuum system. The presence of oxygen can have have two main effects: it may provide background counts from the $^{16}O(\alpha,\gamma)^{20}Ne$, $^{17}O(\alpha,n)^{20}Ne$, and $^{18}O(\alpha,n)^{21}Ne$ reactions; and it will decrease the stopping power per ^{28}Si atom, thereby reducing the yield from $^{28}Si(\alpha,\gamma)^{32}S$ (the stopping power is discussed in Section IC).

The oxygen content was determined by comparing the yield for the $^{16}O(\alpha,\gamma)^{20}Ne$ resonances at 1116 and 1319 keV, from

the 20 keV ^{28}Si target, with that from a thick, fused quartz target (SiO_2). The target composition was found to be $SiO_{0.35\pm0.08}$. As a further check, the lowest resonance found in $^{28}Si(\alpha,\gamma)^{32}S$, at 1776 keV, was measured with both the 20 keV ^{28}Si target and the thick quartz target, and the yields were compared. Although the presence of 4 and 6 MeV γ rays, from the two resonances in $^{16}O(\alpha,\gamma)^{20}Ne$ just mentioned, somewhat impaired the precision of the test, the result supported the value determined from the measurements of the oxygen yield. Of course, these $^{16}O(\alpha,\gamma)^{20}Ne$ resonances did not hinder the $^{28}Si(\alpha,\gamma)^{32}S$ measurements on the ^{28}Si target, because the target was thin enough that the α particles were through it well before reaching the lower energies of these resonances.

B. Excitation Function

The excitation function for the $^{28}Si(\alpha,\gamma)^{32}S$ reaction, measured for bombarding energies from 1.40 to 2.61 MeV, is shown in Figure 9. As indicated in the figure, each datum represents the yield measured for 3000 μC of integrated beam, after the removal of the contribution from natural background (beam independent). The windows for the sum mode and coincidence yield measurements will be described shortly.

The resonance reported by Smulders at 2618 keV was also measured; its peak, for 3000 μC of integrated beam, would have been about 25000 counts, so it is not shown in the figure.

FIGURE 9: Excitation Function for $^{28}Si(\alpha,\gamma)^{32}S$

The excitation function is shown for bombarding energies from 1.4-2.61 MeV, after removal of the contribution from natural background. The thick silicon target was used for the energy range 1.4-1.7 MeV (arrow 1), and the 20 keV ^{28}Si target was used for higher energies. The discontinuity in the sum mode yield at arrow 2 was caused by resetting the sum mode window to eliminate some of the contribution from contaminant reactions. The targets are described in the text, as are the sum mode and coincidence methods. The peaks at 1776, 1995, 2187, 2370, and 2415 keV were identified with the $^{28}Si(\alpha,\gamma)^{32}S$ reaction. The other yield was attributed to the contaminant reactions, $^{13}C(\alpha,n)^{16}O$, $^{10,11}B(\alpha,n)^{13,14}N$, and $^{18}O(\alpha,n)^{21}Ne$. The energies and total widths of the contributing resonances in these reactions are listed in Table 1. For the sum mode windows, the natural background was roughly about 100 counts per run. Therefore, the statistical error on a point showing N corrected counts was $\approx (N+100)^{1/2}$. Lines connecting some of the data are intended only as a guide to the eye.

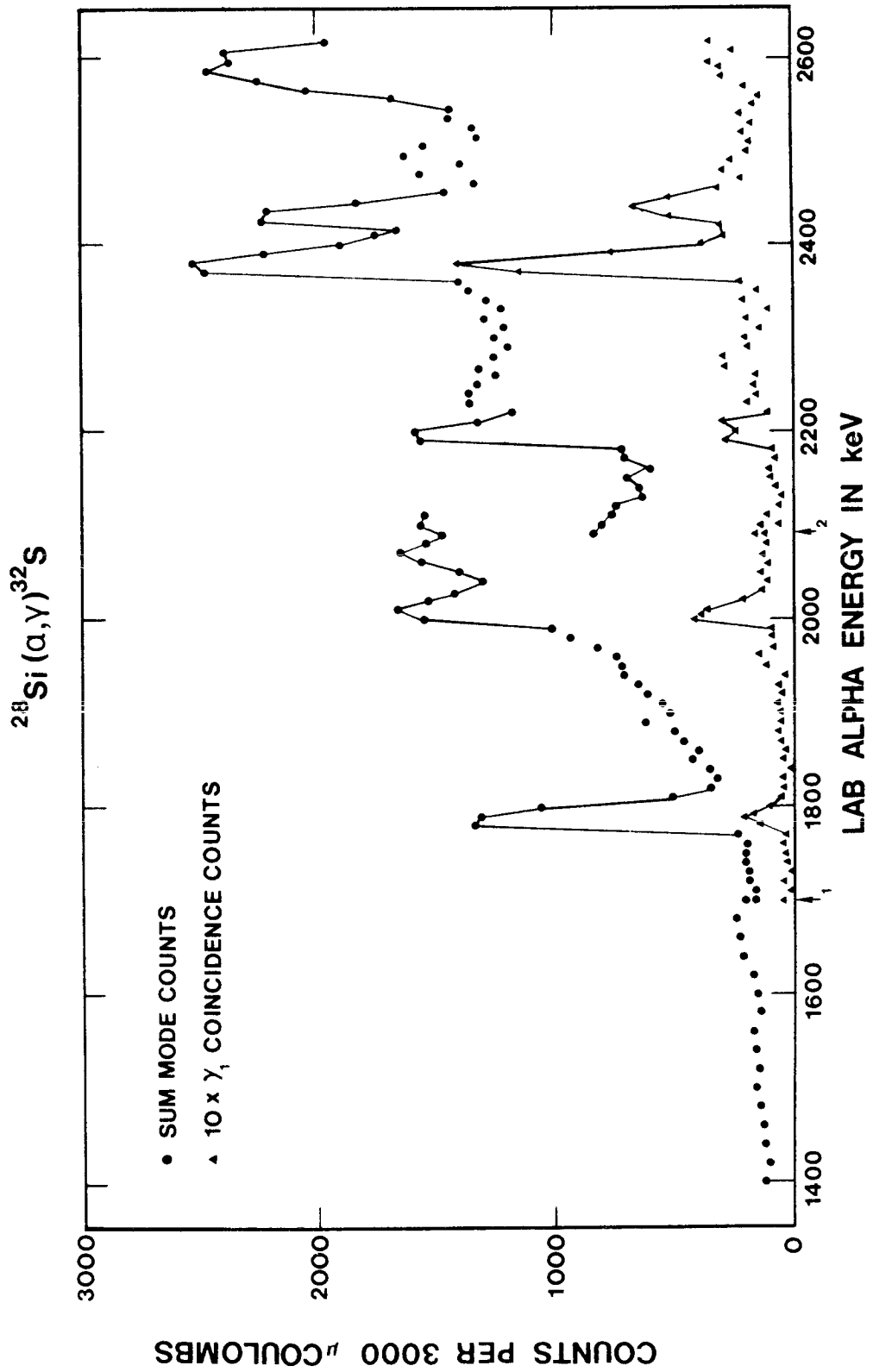
$^{28}Si\ (\alpha,\gamma)^{32}S$
• SUM MODE COUNTS
▲ 10 x γ_1 COINCIDENCE COUNTS
COUNTS PER 3000 μCOULOMBS
LAB ALPHA ENERGY IN keV
0
1000
2000
3000
1400
1600
1800
2000
2200
2400
2600
E_1
E_2

A brief search above this resonance, accumulating 600 uC per run, and using 10 keV intervals between runs, showed no further resonance structure up to 2.75 MeV; these results also are not displayed.

The stopping target (natural silicon) was used for the region 1.4-1.7 MeV, so the points in this region represent the total reaction yield for all energies below the incident beam energy. The intervals between data in this region were 20 keV.

The 20 keV ^{28}Si target and 10 keV intervals were used for all the work at higher energies. One advantage of this thin a target is that the yield, from contaminants within the target, is integrated over only a small energy region ($\approx$20 keV).

The yield curves from both the sum mode and coincidence circuits (described in Section IIB) are displayed. For energies below 2.1 MeV, the SCA window in the sum mode circuit admitted pulses corresponding to energies of 6.0-9.7 MeV. At the energy indicated by the arrow labeled "2" in the figure, the window threshold was raised so that fewer counts from the contaminant reactions (mainly (α,n) reactions) would be counted. This explains the discontinuity in the yield curve. The new window corresponded to 6.9-9.7 MeV. The coincidence circuit was set to detect the two gamma rays resulting from the decay of the resonance level to the 2.24 MeV first excited state of ^{32}S (γ_1 transition), so the upper window on each NaI crystal admitted 6.0-7.5 MeV pulses, and the lower window admitted 2.0-2.5

MeV pulses. For the sum mode windows, the natural background was, very roughly, about 100 counts per run. The statistical error on a point showing N corrected counts, then, was approximately $(N + 100)^{1/2}$.

Several peaks and regions of high yield were attributed to (α,n) reactions on contaminants for the following reasons:

1) the peaks and regions were broad (one expects (α,γ) reactions at these energies to be narrow since the α and γ widths are small and no other channels are usually open; the (α,n) reactions, however, tend to have large neutron widths)

2) they showed little or no evidence for γ_1 transitions expected from the reaction being measured

3) they occurred at energies corresponding to known resonances in (α,n) reactions on expected contaminants, had approximately the correct widths, and were consistent; that is, all the strong resonances in this energy region for a particular reaction were present.

From these considerations, yield was attributed to the resonances listed in Table 1, in (α,n) reactions on the nuclei $^{10,11}B$, ^{13}C, and ^{18}O. The resonance energies and widths in the table were taken from Bonner et al. (1956). The presence of these contaminants was expected: oxygen has been discussed already; carbon buildup on targets is an old, common problem;

TABLE 1: Resonances in Contaminant Reactions in $^{28}Si(\alpha,\gamma)^{32}S$ Yield

Reaction	Resonance Energy	Total Width, Γ
$^{13}C(\alpha,n)^{16}O$	2.09 MeV	100 keV
	2.25	100
	2.42	80
	2.605	$\leq$6
$^{10}B(\alpha,n)^{13}N$	2.16	30
	2.26	200
$^{11}B(\alpha,n)^{14}N$	2.06	59
	2.60	100
$^{18}O(\alpha,\gamma)^{21}Ne$	2.21	30
	2.47	$\leq$15
	2.56	25

The resonance energies and widths were taken from Bonner et al., (1956).

and boron had been detected earlier through the $^{10}B(\alpha,p_3\gamma)^{13}C$ reaction at 1640 keV. It was assumed that the several isotopes of each contaminant were present in their natural abundances.

C. Resonances in $^{28}Si(\alpha,\gamma)^{32}S$

Five resonances, apparently narrow and showing evidence of the appropriate γ_1 transition, were thought to belong to this reaction, and were further investigated. These appear in the excitation function at energies of 1776±5, 1995±5, 2187±7, 2370±4, and 2415±5 keV. The assistance of the γ_1 coincidence technique in identifying these resonances is evident. Long runs directly above and beneath each resonance were taken to provide 400 channel spectra, from which the resonance strengths could be calculated, and from which some qualitative information about the cascade structures might be obtained. To the accuracy with which the gamma energies could be determined, the high energy cutoff in each spectrum corresponded to that expected for the ^{32}S excitation at that bombarding energy, and all of the strong gammas seen in the spectra could be identified with transitions between known levels in ^{32}S.

Each of the resonances was fairly close to a resonance in the $^{24}Mg(\alpha,\gamma)^{28}Si$ reaction, for which the resonance energies in this region have been measured to 2 or 3 keV, as listed in Endt and Van der Leun (1967). Assuming that the fluxmeter in the 90° analyzing magnet could determine energy differences

of up to 40 keV accurately, the resonance energies were determined with a target assembly that had the 5 keV ^{28}Si target on one side, and a 30 keV, natural magnesium target on the reverse side. The target was moved to a fresh spot after each resonance was traced out, to insure that carbon buildup would not affect the calibration. The energies and uncertainties listed in the previous paragraph were determined in this way. The measured resonance energies and the corresponding ^{32}S excitations appear in the first two columns of Table 2. The lowest energy resonance, at 1776 keV, has an excitation energy of 8.50 MeV, and is probably the level listed by Endt and Van der Leun (1967) at 8.496±15 keV, which was seen in the cascade structure of the $^{31}P(p,\gamma)^{32}S$ reaction, and in the $^{31}P(\tau,d)^{32}S$ and $^{32}S(e,e')^{32}S$ reactions. The other 4 resonances correspond to levels that have not been observed or confirmed previously.

Because the resonances are so weak, careful identification with the $^{28}Si(\alpha,\gamma)^{32}S$ reaction must be made. The following paragraphs describe the analysis used for their identification.

The Q value and the low lying ^{34}S levels are remarkably similar in nature to those of ^{32}S, and the γ decays in ^{34}S are not hindered by the isotopic spin selection rule, forbidding T=0 to T=0 transitions for the T=0 levels of self-conjugate ^{32}S. Although the isotopic enrichment should have eliminated the possibility that any of the 5 resonances was

from α-capture on ^{30}Si, as a precaution, the thick target step for each resonance was traced out on the stopping target (natural silicon). If a resonance had been in $^{30}Si(\alpha,\gamma)^{34}S$, its yield would have been enhanced by about a factor of 100; however, after correcting for the oxygen dilution of the ^{28}Si target and the isotopic dilution of the stopping target, the yield from each resonance reproduced quite well. This, incidentally, also provides evidence that the ^{28}Si target was qualified for the thick target approximation (Section IC) for each of the resonances studied, and that the effects of channeling could be neglected for the crystalline target.

The fact that the shape of each resonance peak depends on the target thickness, as seen by comparing the peaks for the 5 keV, 20 keV, and stopping targets, is submitted as proof that the reaction responsible for each resonance occurs in the target material, and not elsewhere, such as in the target backing, chamber walls, or upstream collimators. The spectra verify that the counts are caused by gamma rays, and not by neutrons. A search of the review articles by Ajzenberg-Selove and Lauritsen (1959, 1968), and by Endt and Van der Leun (1967), show that no particle reaction, such as $(\alpha,p\gamma)$, for targets up to at least $A = 40$, can produce γ rays of the energies observed, and the upper limits on impurity concentrations in the ^{28}Si target rule out any radiative capture reactions as the source. It also

seems most improbable that the ^{28}Si targets, evaporated from amorphous Si that had been reduced from SiO_2, and the stopping target, of very pure semiconductor silicon, would have identical impurity concentrations.

Finally, there was a remote possibility that deuterons could have contaminated the beam, since the magnet would not discern between He^+ atoms and D_2^+ molecules of the same energy. To protect against this possibility, the deuterium bottle in the ion source was valved off and isolated from the source by two vacuum seals, and the internal parts of the source (pyrex bottle, quartz sleeve, and canal) were replaced with new parts. The only deuterium present, then, should have been due to the natural abundance of D_2 in the residual hydrogen in the source. The D_2 abundance is about 2.2×10^{-8} molecules per H_2 molecule.

For each resonance, the number of counts in the sum mode SCA window was compared with the number of counts in the portion of the corrected spectrum that corresponded to the sum mode window, and the result was used to correct N_B. This procedure corrects for the possibility that the below-resonance spectrum was not taken completely below the resonance, or that the above-resonance spectrum was not measured on the yield plateau. The resonance strengths were calculated with the method outlined in Section IVB. The resonance energies, excitation energies, and total strengths for the resonances appear

in the first three columns of Table 2. The fourth column indicates any apparent qualitative features of the cascade structures. The strength of the resonance reported by Smulders (1964) was also measured here, and this result is included in the table. Smulders quoted a strength that is approximately 1/2 of the value obtained here, but he measured only the strengths of the γ_0 and γ_1 transitions. The spectrum shows some evidence for decays to higher states, so this disagreement is probably not important.

The uncertainties tabulated for the resonance strengths came from two main sources:

1) the uncertainty in $\mathcal{E}$ is estimated at 12 - 15%, which includes uncertainties in values for $\mathcal{E}$ in the literature plus uncertainty in the correction for oxygen contamination;

2) the uncertainty in N_γ was a combination of the statistical error in N_B (small) and the uncertainty in η, which depended on the "cleanliness" of the individual spectra, and therefore on the background at the resonance energies.

Spectra for the six resonances appear in Figures 10 - 15. The arrow on the abscissa in each figure indicates the starting channel for the integral that determined N_B. The quantities f and $\eta(f)$, used to determine N_γ, are described in the captions, and the various peaks in the spectra are identified.

TABLE 2: Resonance Energies and Strengths for $^{28}Si(\alpha,\gamma)^{32}S$

Resonance Energy (keV)[a]	^{32}S Excitation (MeV)	$(2J+1)\Gamma_\alpha\Gamma_\gamma/\Gamma$ (eV)[a]	Comments on Cascade Structure (from spectra)
1776±5	8.50	0.025±0.007	Strong γ_0; $\gamma_0/\gamma_1 \approx 8$
1995±5	8.69	0.020±0.006	Strong γ_1; $\gamma_1/\gamma_0 \approx 2$
2187±7	8.86	0.041±0.014	Strong γ_1; $\gamma_1/\gamma_0 \approx 2$
2370±4	9.02	0.093±0.023	Strong γ_1; $\gamma_1/\gamma_0 \approx 3$, $\gamma_1/\gamma_3 \approx 2$
2415±5	9.06	0.134±0.034	Strong γ_7; $\gamma_7/\gamma_1 \approx 4-5$
2618±4	9.24	0.61 ±0.15	Strong γ_1; $\gamma_1/\gamma_0 \approx 3$, $\gamma_1/\gamma_2 \approx 2$
(2581)	9.207	< 0.015	
1400 - 1700		< 0.0008	
< 1400		< 0.0001	

[a]Measured in Lab Units

FIGURE 10: Spectrum for the 1776 keV Resonance in $^{28}Si(\alpha,\gamma)^{32}S$

The spectrum shows a peak in channel 350, indicating a strong γ_0 transition. This peak actually consists of two peaks; one is the full energy peak for this gamma ray, and the otherwas caused by a pair event, in which one of the 0.511 MeV annihilation quanta escaped the NaI. This is the cause of the "double-humped" shape, which is typical for γ rays of this energy. Throughout these figures, the channel numbers and energies will refer to only the full energy peaks.

Evidence for a weak γ_1 transition is found in the peak at 6.26 MeV (channel 215). The peak in channel 150 was probably caused by both a 3.85 and a 3.78 MeV gamma. The 3.85 MeV gamma was contributed by the 1830 keV resonance in $^{10}B(\alpha,p_3\gamma)^{13}C$, whose width is $\Gamma=35\pm8$ keV (Gallmann et al., 1969). The 3.78 MeV γ ray was from $^{28}Si(\alpha,\gamma)^{32}S$; further evidence for the transition to the 3.78 MeV level in ^{32}S is provided by a possible peak near channel 200, and the 1.54 and 2.24 MeV peaks (channels 65 and 90), which would be produced by the decay of the 3.78 MeV level through the first excited state. The uncertainty caused by the $^{10}B(\alpha,p_3\gamma)^{13}C$ contribution was considered in the calculation of N_B. The parameters used to calculate N_γ were $f=0.35$, $\eta=0.35$, and the arrow indicates the starting channel.

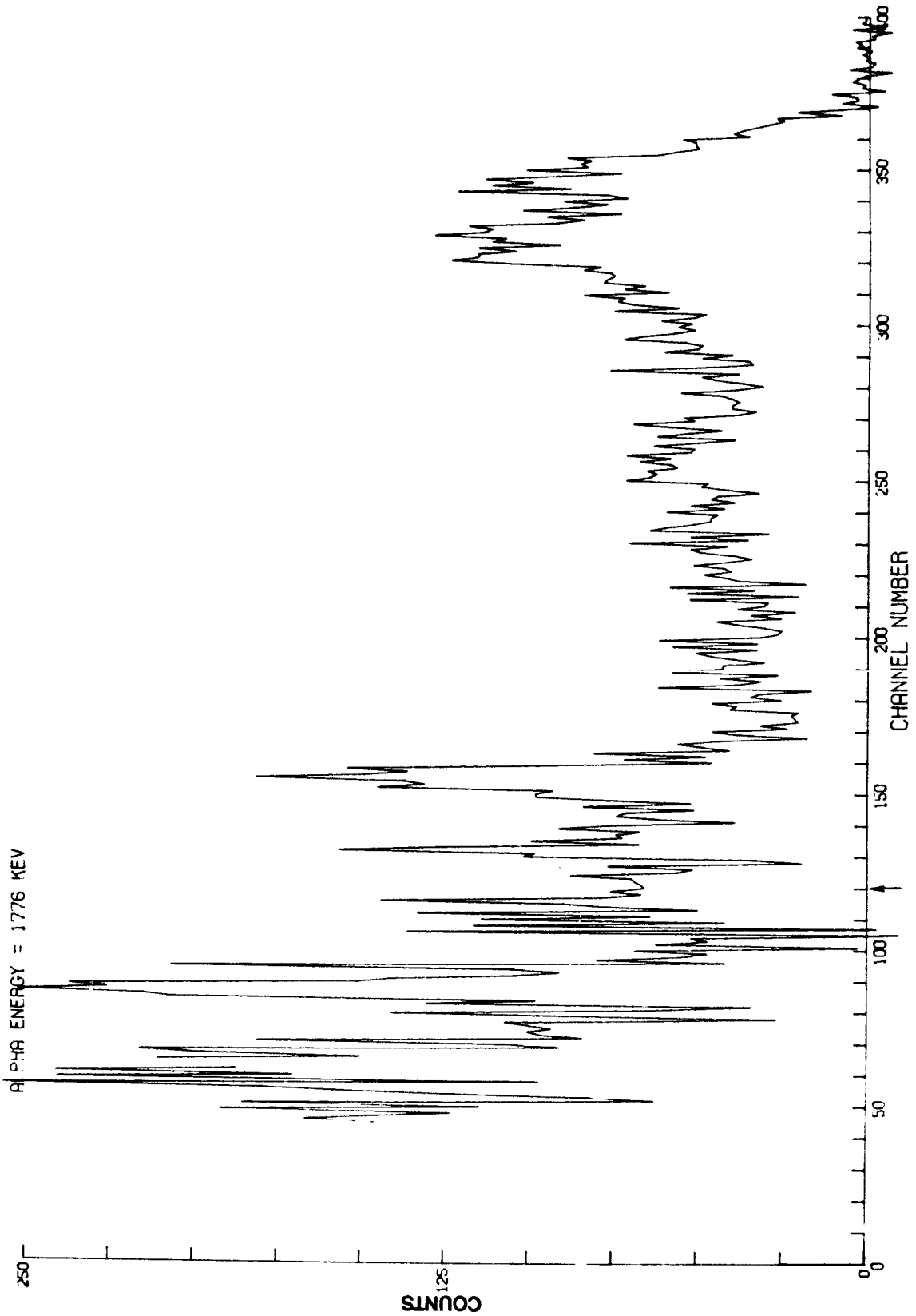
ALPHA ENERGY = 1776 KEV
COUNTS
250
125
0
0
50
100
150
200
250
300
350
400
CHANNEL NUMBER

FIGURE 11: Spectrum for the 1995 keV resonance in $^{28}Si(\alpha,\gamma)^{32}S$

The only identifiable peaks, near channels 260 and 350, correspond to γ_1 and γ_2 transitions. The low energy portions of the spectrum were obscured by neutrons, probably from the $^{11}B(\alpha,n)^{14}N$ reaction. The parameters were f=0.45 and η=0.26±25%.

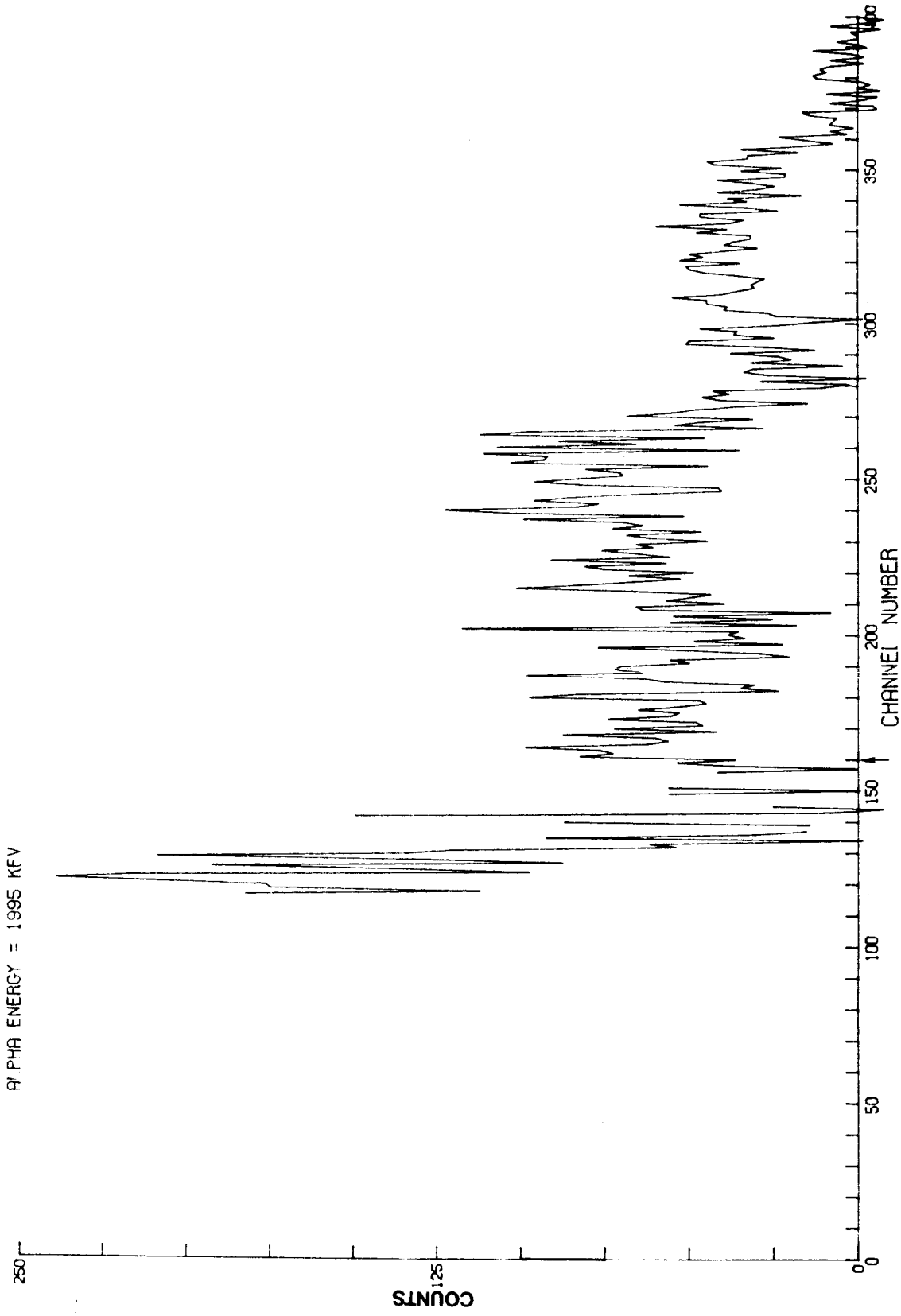
ALPHA ENERGY = 1995 KEV
COUNTS
250
125
0
0
50
100
150
200
250
300
350
400
CHANNEL NUMBER

FIGURE 12: Spectrum for the 2187 keV Resonance in $^{28}Si(\alpha,\gamma)^{32}S$

The high energy members of the γ_0, γ_1, and possibly γ_2 transitions would appear near channels 355, 265, and 205, respectively. The low energy contamination was probably caused by the $^{13}C(\alpha,n)^{16}O$ reaction. The arrow indicates the starting channel for f=0.44; the value used for η was 0.265±25%.

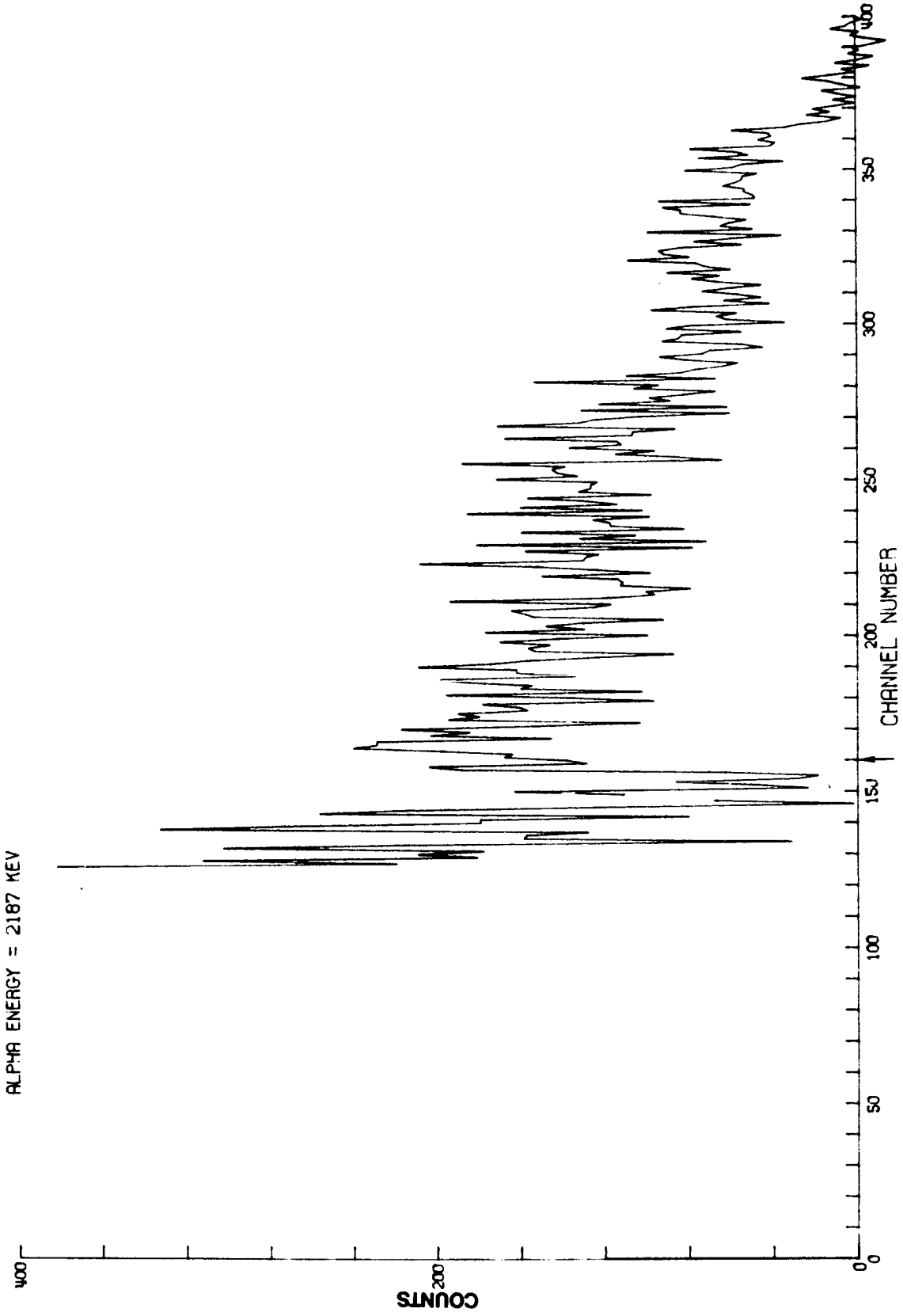
ALPHA ENERGY = 2187 KEV
COUNTS
CHANNEL NUMBER
0
50
100
150
200
250
300
350
400
200
400

FIGURE 13: Spectrum for the 2370 keV Resonance in $^{28}Si(\alpha,\gamma)^{32}S$

Contributions from γ_0, γ_1, and γ_3 are seen in channels 360, 270, and 190, respectively. The arrow indicates a starting channel for the N_B calculation that corresponds to f = 0.41, and the value used for η was 0.285±20%.

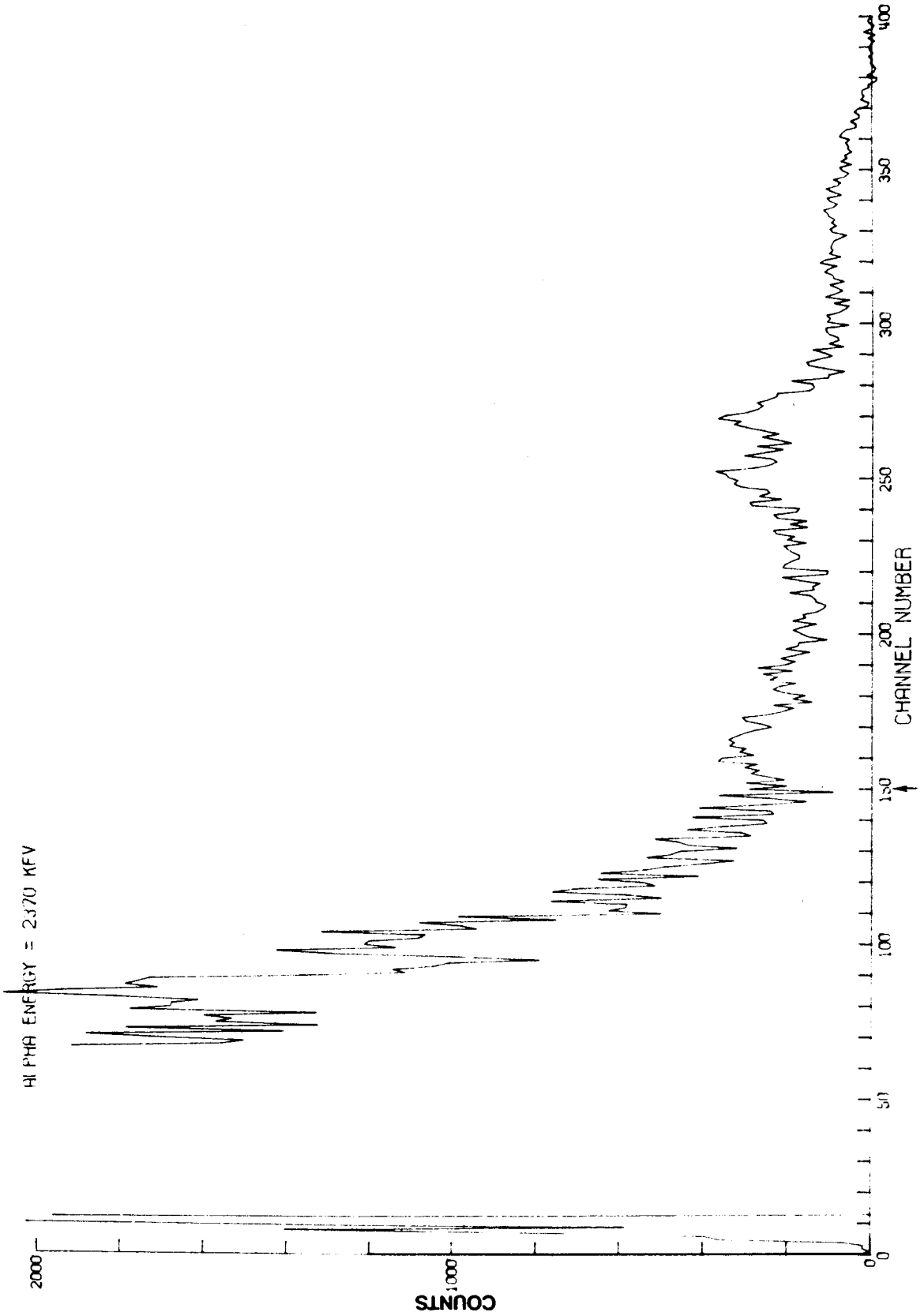
ALPHA ENERGY = 2370 KEV
COUNTS
2000
1000
0
0
50
100
150
200
250
300
350
400
CHANNEL NUMBER

FIGURE 14: Spectrum for the 2415 keV Resonance in $^{28}Si(\alpha,\gamma)^{32}S$

The strongest γ ray corresponds to the γ_7 transition, to the 5.41 MeV level in ^{32}S. This transition provided γ rays of the following energies and origins:

3.6 MeV	Channel 145	E_X - 5.41
3.2	125	5.41 - 2.24
2.24	85	2.24 - 0

There is also evidence in channel 270 for the γ_1 transition. At the arrow, f=0.35, and the value chosen for η, because of the 3γ spectrum, was $\eta = 0.31 \pm 20\%$.

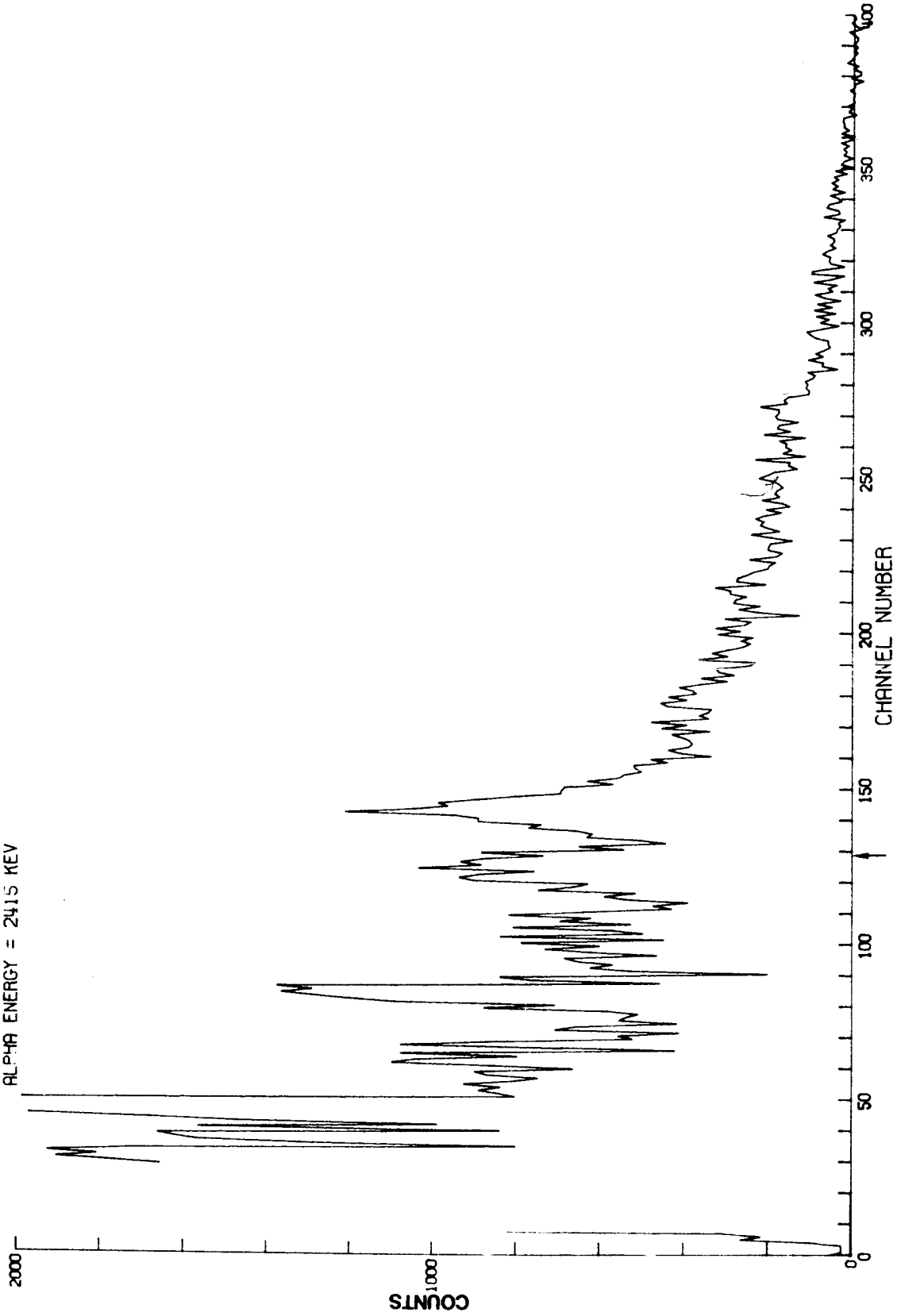
ALPHA ENERGY = 2415 KEV
COUNTS
2000
1000
0
0
50
100
150
200
250
300
350
400
CHANNEL NUMBER

FIGURE 15: Spectrum for the 2618 keV Resonance in $^{28}Si(\alpha,\gamma)^{32}S$

The spectrum shows evidence for the γ_0, γ_1, and γ_2 transitions with peaks in channels 380, 290, and 230. The 2.24 MeV peak is visible in channel 90, and perhaps the peak near channel 60 was caused by a 1.5 MeV gamma from the 3.78 - 2.24 transition. The peak near channel 45 is thought to be from $^{19}F(\alpha,p_1\gamma)^{22}Ne$. The spectrum was over-subtracted for channels below 140 because of the decreasing yield from the $^{18}O(\alpha,n)^{21}Ne$ resonance at 2560 keV, therefore f could be given a value no lower than 0.40 (see arrow), corresponding to $\eta = 0.345 \pm 20\%$.

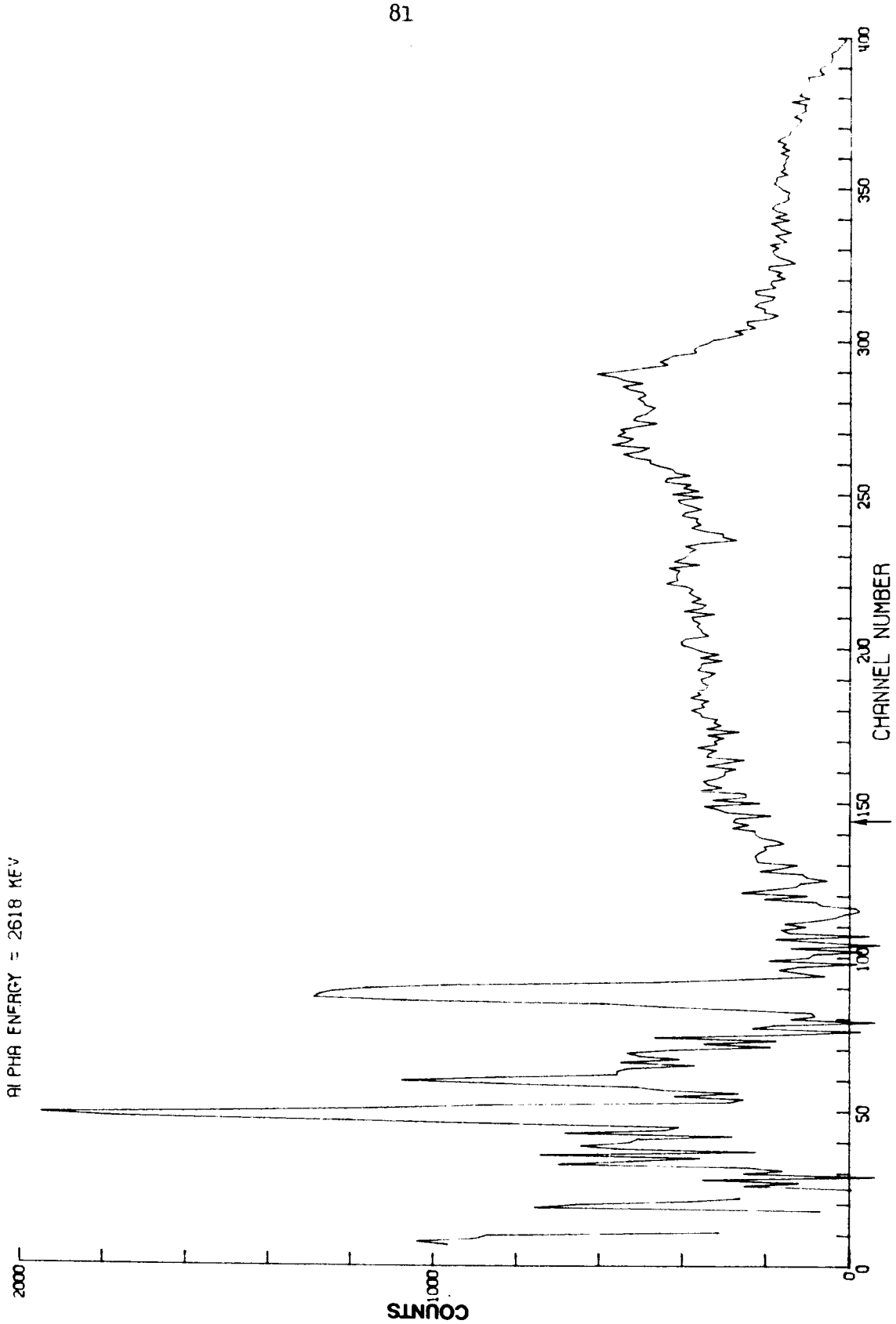
ALPHA ENERGY = 2618 KEV
COUNTS
2000
1000
0
0
50
100
150
200
250
300
350
400
CHANNEL NUMBER

D. Upper Limits to Resonance Strengths

Upper limits were established for the resonance yield in three energy regions, using different procedures in each region. The procedures and results will be discussed in the following paragraphs.

1. $E_{He^+} = 2581$ keV

A level in ^{32}S at 9.207 MeV has been found in the $^{31}P(p,\gamma)^{32}S$ reaction, and the branching ratios for its cascade members have been measured (Endt and Van der Leun, 1967). The level has been shown to have J=1, but its parity has not been determined, so the level possibly could be formed in the $^{28}Si + \alpha$ system. The excitation of this level would correspond to a bombarding energy of 2581 keV in the $^{28}Si(\alpha,\gamma)^{32}S$ reaction. Competition from contaminant reactions in this region rendered the sum mode useless for the study of this level, but it has a branching ratio of 38% for the γ_1 transition, and could therefore be detected with the coincidence system. The γ_1 branching ratio for the 2370 keV resonance was estimated to be (55±10)% from the spectrum for this resonance, and its strength had been determined with the sum mode system. The upper limit to the strength of the 2582 keV resonance, S_{2582}, was calculated simply by comparison to the 2370 keV resonance strength, S_{2370}, as follows:

$$S_{2582} < \frac{(55 \pm 10)\%}{38\%} \frac{C_{2582}}{C_{2370}} S_{2370}, \qquad (26)$$

where C_{2370} was the coincidence yield for the 2370 keV resonance, and C_{2582} was the upper limit to the coincidence yield for the 2582 keV region. The result, which also appears in Table 2, was $(2J+1)\Gamma_\alpha\Gamma_\gamma/\Gamma < 0.015$ eV. Although this is not a particularly good limit, it is small enough that any astrophysical contribution at 2582 keV can be neglected in view of the stronger surrounding resonances.

2. 1400-1700 keV

For bombarding energies in the region, 1.4-1.7 MeV, a careful study of the excitation function measured by the sum mode system provided an estimate of the smallest step that could be detected. This estimate was compared with the yield from the 1776 keV resonance, which allowed an upper limit of $(2J+1)\Gamma_\alpha\Gamma_\gamma/\Gamma < 0.0008$ eV to be placed on the strength of any resonance in this energy range. A small step in the yield at 1640 keV prompted long spectrum runs above and below this energy. A very strong 3.85 MeV gamma ray from the resonance in $^{10}B(\alpha,p_3\gamma)^{13}C$, at 1640 keV, suggested that the level formed in the compound nucleus (^{14}N) had a large enough electromagnetic decay width to provide the gamma rays in the 6 - 9 MeV range that were observed in the yield step. The excitation and spin of this level in ^{14}N, and the cascade structure seen from nearby

levels of the same spin and parity, support this theory.

3. $E_{He^+} < 1400$ keV

A long run at 1400 keV on the stopping target allowed an upper limit to be placed on the strength of any resonance at an energy below 1400 keV. It was argued that any yield above 8.67 MeV, 0.5 MeV above the ^{32}S excitation corresponding to 1400 keV bombarding energy, must be from a contaminant reaction. Assuming that the contaminant contribution had a fairly flat shape, an average yield per channel was calculated for the region in the spectrum above 8.67 MeV, and was subtracted from each channel in the region admitted by the SCA window. After this correction (and the usual natural background correction), the net yield in the channels corresponding to the window was 3 ± 32 counts in 45000 μC of integrated beam. Comparing this with the yield from the 1776 keV resonance provided an upper limit of 0.0001 eV for $(2J+1)\Gamma_\alpha \Gamma_{\gamma_1+\gamma_0}/\Gamma$; This result also appears in Table 2.

VI. THE $^{16}O(\alpha,\gamma)^{20}Ne$ REACTION

A. Targets

The $^{16}O(\alpha,\gamma)^{20}Ne$ reaction was investigated with the spectrometer, using the prescription discussed in Section IVA for the calculation of N_γ. Because it was desired to measure a very small reaction yield, careful consideration was given to the selection of target material. If the material is a chemical compound, the elements other than oxygen should not have a very low Z, yet the material should contain as much oxygen, by weight, as possible, so that the stopping power per oxygen atom will be large. The material should also be available in a very pure form, particularly with regard to low Z contaminants, and it should be rugged enough to withstand high beam currents. This last quality requires an optimum combination of high melting point and high thermal conductivity.

Fused quartz, SiO_2, best fitted the requirements. An O_2 target would of course offer the highest yield, but gas targets present other problems. The entrance window on a closed cell must be extremely thin if it is to pass low energy α particles, but such a thin foil would not withstand the large beam currents that are necessary for very low yield measurements. A differentially pumped gas system would be too ungainly to allow the

close placement of the NaI detectors, so that detection efficiency, and therefore yield, would be sacrificed. The next two suitable compounds, in order of stopping power, are silica (of which fused quartz is the most common form in the laboratory), and water; the stopping power per oxygen atom for each of these is 5/8 of the stopping power for oxygen. Although ice targets have been used, they present difficulties; therefore, fused quartz was chosen.

Two targets were used. The first, a rectangular piece of quartz approximately 1/8 inch thick, was used to obtain the spectra for the 1116 and 1319 keV resonances. Because of the low thermal conductivity of quartz (one requirement not met), the beam spot became very hot, which helped to keep the target free from the deposition of hydrocarbon vapors. However, for beam power above a certain limit, the quartz became too hot, and melted fairly rapidly. For a 3/16 inch beam spot, and a 1 MeV bombarding energy, this limit was about 10 microamperes of He^+ ions. In addition, the dielectric property of the quartz kept the accumulated charge from dissipating. On one long run, the quartz developed a tiny fracture through which the front surface discharged to a metal clip that supported the quartz. The discharge occurred at intervals of several seconds, accompanied by radiation that produced numerous spurious pulses in the counting systems. The problem of discharge was remedied by placing a sharp sewing needle very close to the beam spot, but

outside the path of the beam, allowing a coronal discharge to the point.

Because of the thermal and electrical problems associated with bulk quartz, a second target was fabricated and used for the long runs at 1000 and 850 keV. A piece of very high purity quartz, manufactured by Amersil, Inc. (Los Angeles), was fractured with a clean hammer, and the small grains were then evaporated, in vacuum with electron beam bombardment, onto a copper block that could be water cooled in the target chamber. The thickness of the evaporated quartz layer was roughly equal to the range of an 800 keV α particle, and was measured by tracing out the yield shape for the 1319 keV resonance, monitoring the γ_1 yield with the coincidence system. Information obtained from the manufacturer indicated that the quartz contained 1.3 parts per million by weight of Li_2O, and less than 0.1 parts per million by weight boron.

B. The Resonances at 1116 and 1319 keV

Spectra for the 1116 and 1319 keV resonances were measured with the thick quartz target, using the sum mode electronics. At the same time, the coincidence system monitored the γ_1 transitions, providing information that was useful elsewhere in the study. The spectrum for the 1319 keV resonance is shown in Figure 16. This spectrum is the difference of two spectra

FIGURE 16: Spectrum for the 1319 keV Resonance in $^{16}O(\alpha,\gamma)^{20}Ne$

The full energy peaks for gamma rays of energy 1.63, 4.16, and 5.79 MeV appear in channels 80, 210, and 390, respectively. The first escape peaks for the latter two gamma rays are also visible, and the counts between the peaks are from gamma interactions via the Compton scattering process. These gamma rays originated in γ_0 and γ_1 transitions; their branching ratios for this level are $(18\pm5)\%$ and $(82\pm5)\%$, respectively (Van der Leun et al., 1965). Beneath channel 100, the number of counts was determined by extrapolating horizontally from channel 100 to channel 0, measuring the number of counts in the full energy peak of the 1.63 MeV gamma ray, and converting this to the total number of 1.63 MeV counts with the aid of a photofraction obtained for this gamma ray from the gamma spectrum for $^{23}Na(p,\alpha_1\gamma)^{20}Ne$. The spectrum shown in the figure is the difference of two spectra measured just above and just below the 1319 keV resonance, and it has been corrected for natural background.

The numbered arrows indicate boundaries of the regions used in the analysis of the 1000 and 850 keV runs.

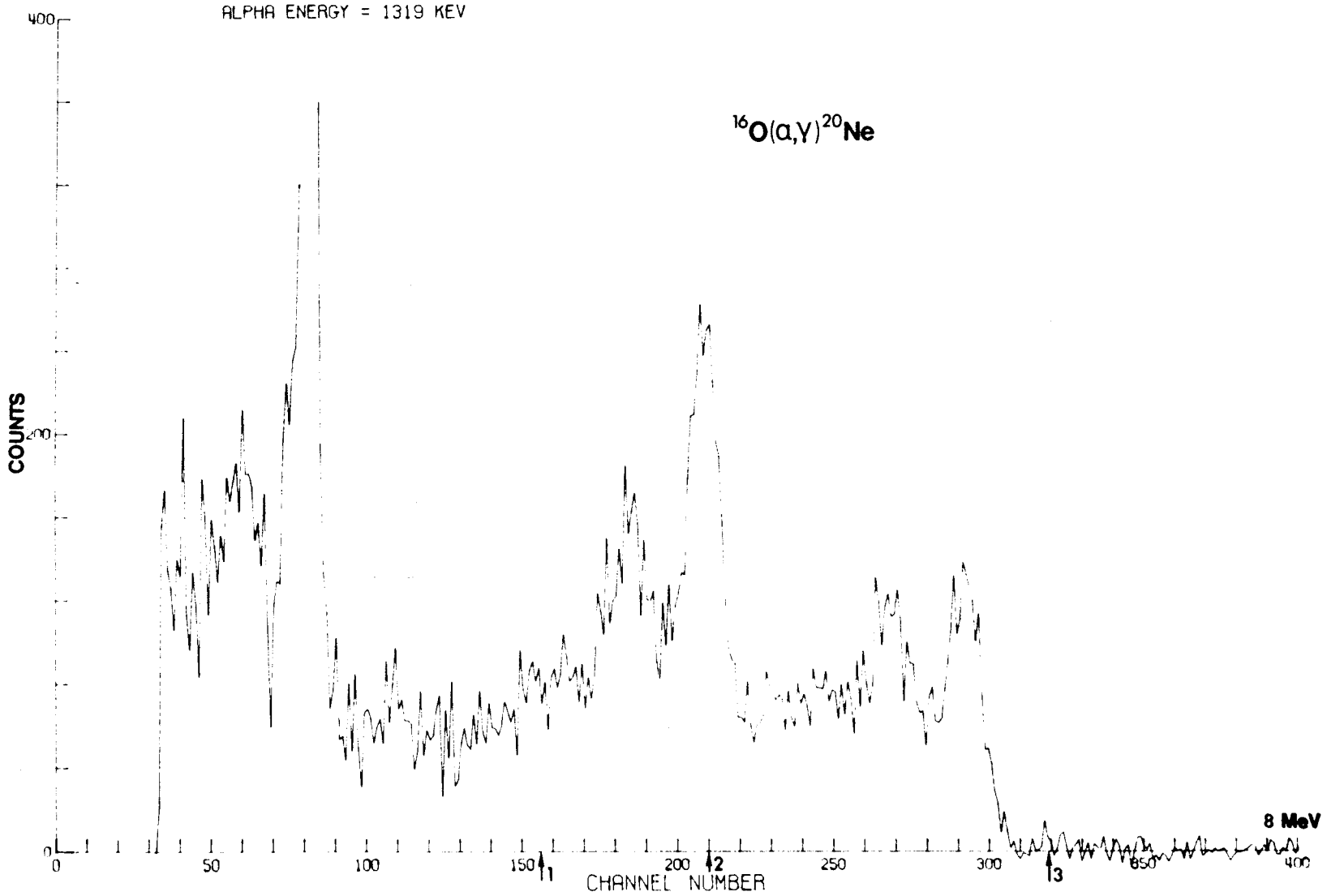
ALPHA ENERGY = 1319 KEV
$^{16}O(\alpha,\gamma)^{20}Ne$
COUNTS
400
200
0
0
50
100
150
200
250
300
350
400
1
2
3
8 MeV
CHANNEL NUMBER

measured just above and just below the 1319 keV resonance; the contribution from natural background has been removed. Although this resonance is as weak as the weakest resonance observed in $^{28}Si(\alpha,\gamma)^{32}S$, the lower energy produced far fewer counts from contaminant reactions, and the improvement of the spectrum is dramatic.

For each resonance, N_γ was determined in two separate ways. The first method included the contribution from the 1.63 MeV γ ray by measuring the number of counts contained in its peak, and then dividing that number by the photofraction for a 1.63 MeV gamma (the photofraction is defined as the ratio of the contribution in the full energy peak to the total contribution in the spectrum from the γ ray). The photofraction was determined from a 1.63 MeV gamma spectrum obtained with the $^{23}Na(p,\alpha_1\gamma)^{20}Ne$ reaction.

For the second determination of N_γ, the 1.63 MeV gamma was ignored, and the low energy tail from the more energetic gamma rays was extrapolated horizontally to zero energy. The two values were averaged, and their difference determined the uncertainty assigned to N_γ. The values for the total resonance efficiency, ϵ_T, were calculated using Equation 22, Section IVA, with branching ratios from Van der Leun et al. (1965).

Since the multipolarity of the radiation had been measured by these same investigators for the 4.17 MeV gamma from the

1319 keV resonance, and was otherwise unambiguous, the effects of angular distributions were easily calculated, using the Q_i factors discussed in Section IIIC, and angular distribution coefficients from Pearson (1963). The resonance strengths are listed in Table 3, along with the values measured by Van der Leun et al.(1965--this paper will henceforth be referred to as VSS). The agreement was quite good.

C. The Resonance at 2490 keV

A resonance at 2490 keV was also investigated by VSS, who point out the difficulty arising from the nearby resonance in $^{18}O(\alpha,n)^{21}Ne$ at 2470 keV. Their value for the strength, $(2J+1)\Gamma_\alpha\Gamma_\gamma/\Gamma$, was 33 ± 15 meV, and for the total width, Γ, was 15 ± 7 keV. The evaporated quartz target used in the present experiment was substantially thicker than the target used by VSS, and it therefore integrated even more of the yield from the $^{18}O(\alpha,n)^{21}Ne$ resonance, rendering impossible an investigation of the 2490 keV resonance with the sum mode system. The coincidence system, however proved more useful. VSS list the decay of this level as a pure γ_1 transition, emitting 1.63 and 5.13 MeV gammas in coincidence. Using six SCA units, two with windows set on the 5.13 MeV peak, two set on the 1.63 MeV peak, and two set on a region of similar size just above the 1.63 MeV peak, coincidences between the 5.13 and 1.63 MeV pulses, and between 5.13 and "> 1.63" MeV pulses could be

monitored simultaneously. Since neutron processes could produce coincident pulses in either set of windows, the > 1.63-5.13 pair could independently monitor variation in the yield from (α,n) reactions. The excitation function, measured over the step of the 2490 keV resonance, remained almost flat in the > 1.63-5.13 yield, indicating that the neutron yield was changing quite slowly over this region. The yield step measured in the 1.63-5.13 system was then attributed to γ rays from the 2490 keV resonance of interest. In a manner very similar to that used for placing the upper limit on the strength of the 2581 keV resonance in $^{28}Si(\alpha,\gamma)^{32}S$ (Section VD), the γ_1 yield from the 2490 keV resonance was compared with the γ_1 yield from the 1319 keV resonance, and the strength was determined to be 41±12 meV, in agreement with the value 33±15 meV as measured by VSS. From the shape of the yield step, the width of the resonance was measured to be 10±5 keV, which is also in agreement with the VSS value, 15±7 keV.

D. Yield for $E_{He^+} < 1000$ keV: 1. Sum Mode Results

Very long runs were taken at bombarding energies of 1000 and 850 keV, so that an upper limit for the strength of any resonance below 1000 keV could be calculated. The water cooled, evaporated target was used, and beam currents of 20-30 μamperes were typical. The condition of the target was checked fre-

quently by retracing the yield step of the 1116 keV resonance. The total integrated beam current was 0.46 C and 0.36 C for the 1000 and 850 keV runs, respectively. Clearly the main problem in establishing a good upper limit to the reaction yield is in handling the background counts from natural sources and contaminant reactions. The natural background, due mainly to ^{40}K, ThC", and cosmic rays, was determined accurately by measuring it for 7×10^4 seconds. The spectrum obtained from a similar run appears in Figure 17. The sum window covered channels 156-319, corresponding to energies of 3.1-6.4 MeV. In this window, the count rate due to natural background was 0.469 counts/second.

X-rays from the accelerator terminal could have provided another source of background, but since the counting rate due to the natural background, and to neutrons, was already high enough to render useless that portion of the spectrum below 3 MeV, it was not necessary to correct for the X-ray contribution.

As mentioned previously, neutron background from the $^{13}C(\alpha,n)^{16}O$ reaction was to be anticipated. The yield from this reaction changed with time, depending on the thickness of the deposited carbon layer, and therefore could not be accurately calculated. The shape of the neutron spectrum proved useful, however, and so was measured at several energies,

FIGURE 17: Natural Background Spectrum

This is the spectrum accumulated by the spectrometer in 8×10^4 seconds. The peak near channel 100 is the 2.61 MeV quantum from ThC". Note that for this spectrum, 400 channels corresponds to 10 MeV, whereas the other spectra displayed in connection with the $^{16}O(\alpha,\gamma)^{20}Ne$ measurements used 8 MeV for full scale.

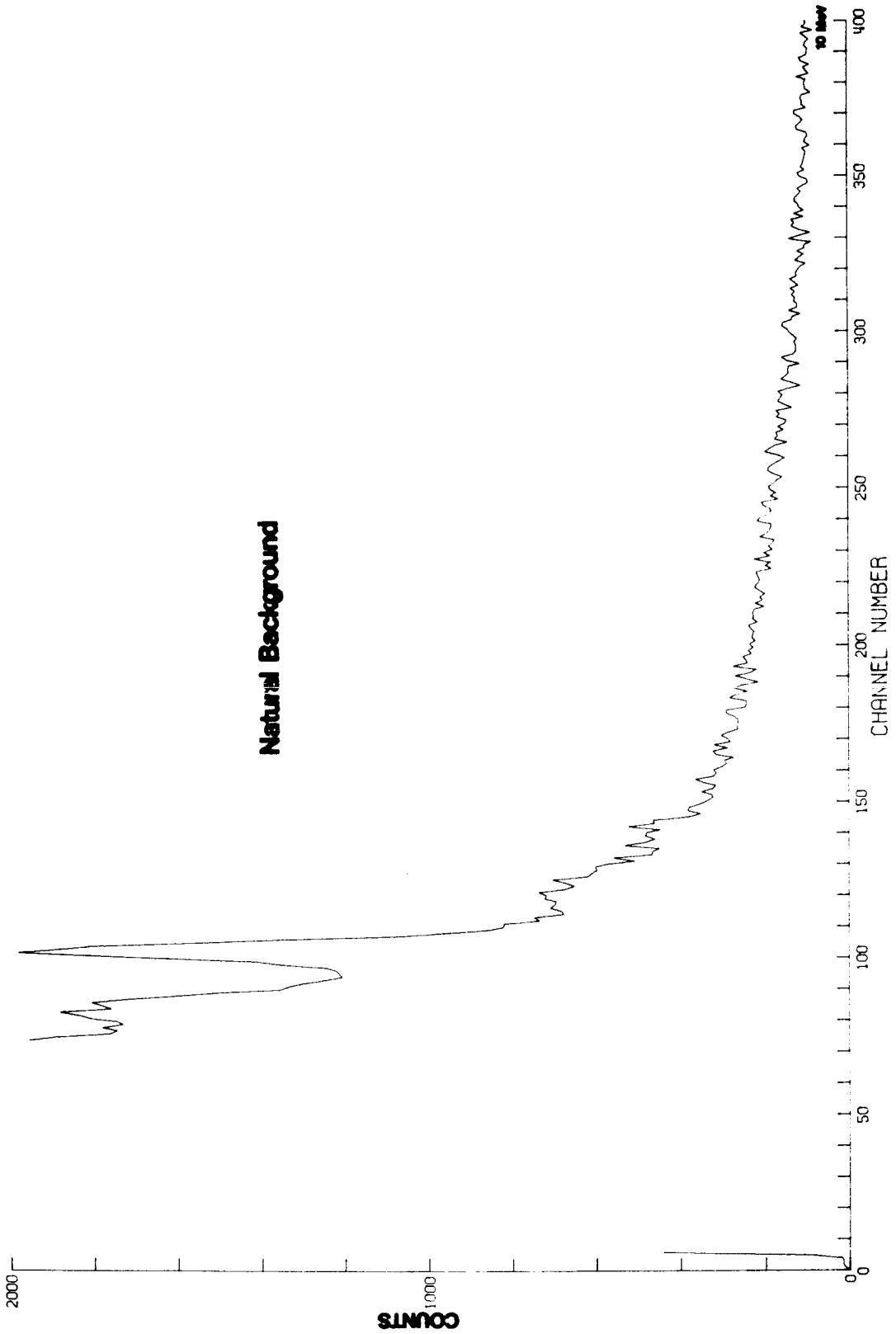
Natural Background
COUNTS
2000
1000
0
0
50
100
150
200
250
300
350
400
CHANNEL NUMBER

including 850 and 1000 keV, with a target of 54% ^{13}C, supplied by Dr. C. N. Davids. The spectrum at 1000 keV is shown in Figure 18.

The importance of boron as a contaminant became clear when the target thickness was determined. Although present in a concentration of less than a part per million, the boron produced a sum mode yield at 1510 keV that equaled the yield from the $^{16}O(\alpha,\gamma)^{20}Ne$ resonance at 1319 keV. Spectra measured at this resonance and at a second resonance at 1640 keV, allowed the yield to be identified with the $^{10}B(\alpha,p_3\gamma)^{13}C$ reaction. The most energetic gamma ray from this is a 3.85 MeV gamma, which is very near the energetic member of the γ_1 transition in ^{20}Ne in this energy region. A natural boron target, consisting of boron powder pressed into a depression in a piece of copper, was used to measure the yield at 1510 keV, 1000 keV, and several other energies of interest. Since the spectrum for the 1510 keV resonance, taken on the quartz target, was clean enough to allow analysis, comparison of the several spectra provided an estimate for the boron yield from the quartz target at 1000 keV. The spectrum measured at 1130 keV from the natural boron target appears in Figure 19.

As mentioned previously, lithium was known to be present in the quartz. From the Q values for the $^{6,7}Li+\alpha$ systems, it can be seen that only the (α,γ) reactions need to be considered for these energies. Furthermore, ^{6}Li accounts for only 7% of

FIGURE 18: Spectrum from the $^{13}C(\alpha,n)^{16}O$ Reaction

The spectrum for this reaction was measured at a bombarding energy of 1000 keV, on a target composed of 54% ^{13}C. The target was approximately 100 keV thick. Pulse pileup was estimated to have contributed less than 2% of the counts in the region between channels 156 and 319. The yield was produced by about 9000 uC of integrated beam current (He^+ ions).

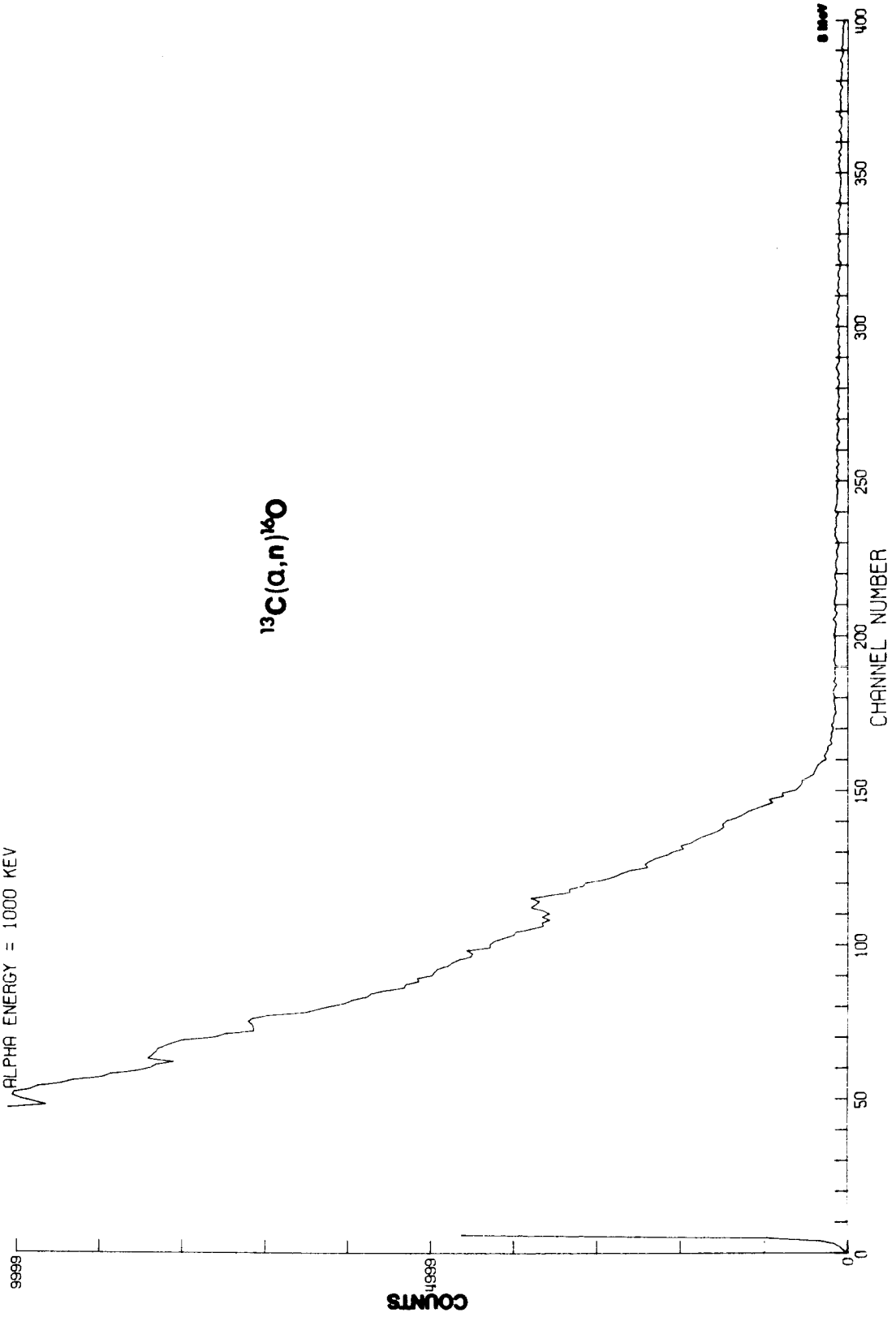
$^{13}C(\alpha,n)^{16}O$
ALPHA ENERGY = 1000 KEV
COUNTS
9999
6666
0
0
50
100
150
200
250
300
350
400
CHANNEL NUMBER

FIGURE 19: Spectrum from the $^{10}B(\alpha,p_3\gamma)^{13}C$ Reaction

This spectrum was measured at a bombarding energy of 1300 keV, where the reaction has a resonance that is 40±5 keV wide (Gallmann et al., 1969). The integrated He^+ beam current was about 90 uC. The target was a pellet of natural boron. The full energy peak and first escape peak for the 3.85 MeV gamma are seen in channels 195 and 170. The hump on the low-energy shoulder of the escape peak was contributed by a 3.09 MeV gamma from $^{10}B(\alpha,p_2\gamma)^{13}C$.

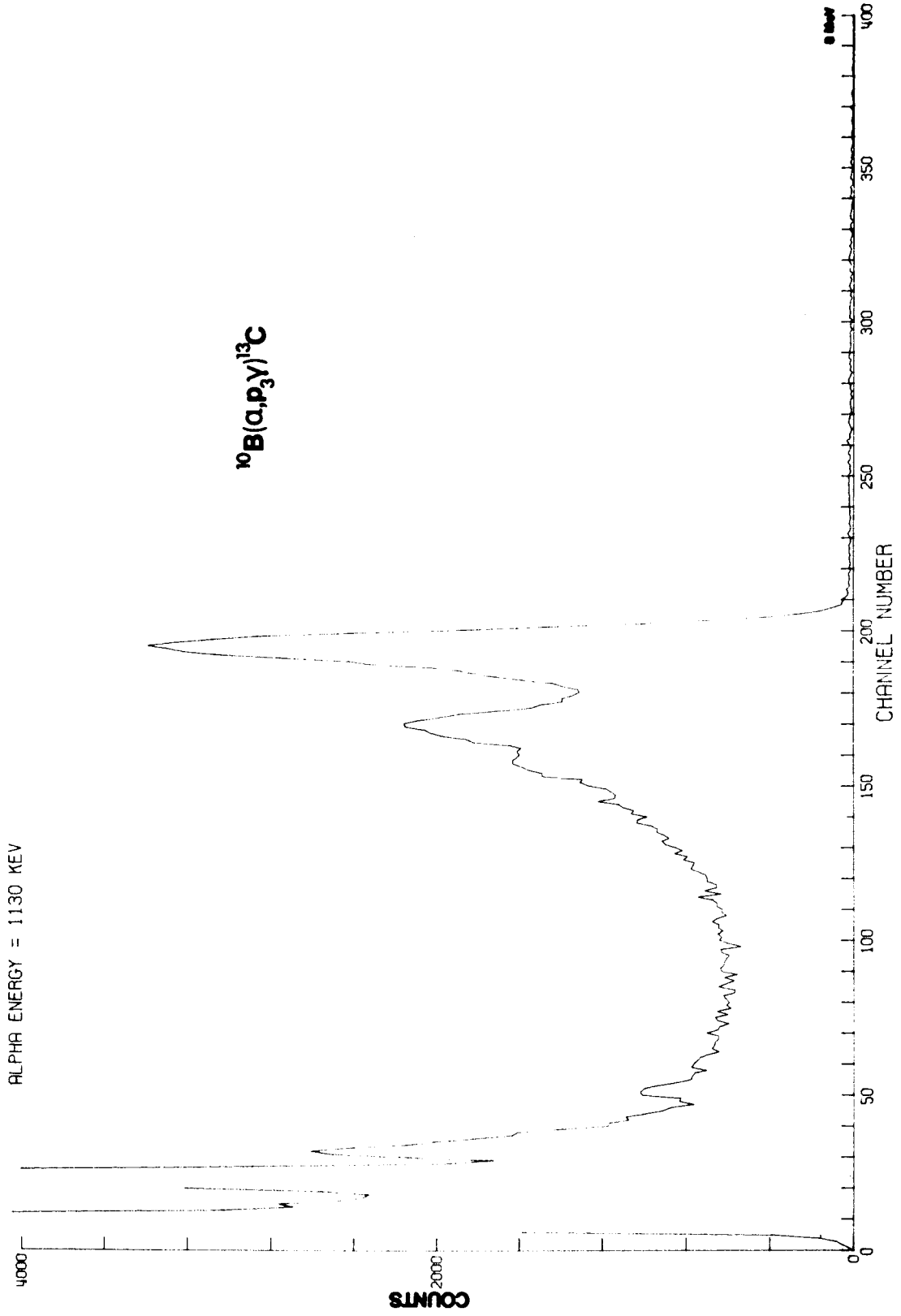
$^{10}B(\alpha,p_3\gamma)^{13}C$
ALPHA ENERGY = 1130 KEV
COUNTS
4000
2000
0
0
50
100
150
200
250
300
350
400
CHANNEL NUMBER

the natural lithium abundance, and the only $^{6}Li+\alpha$ resonance below 1000 keV is weak enough to be neglected (Ajzenberg-Selove and Lauritsen, 1966). Therefore, only the $^{7}Li(\alpha,\gamma)^{11}B$ reaction could have contributed to the background, but since it is a radiative capture reaction on an impurity, it was at first expected to be negligible, and no special measurements were made on lithium targets. It was, however, important in the final analysis, and its contribution there will be discussed shortly.

After the removal of natural background, the spectra obtained from the 1000 and 850 keV runs were of too poor a quality to yield to analysis by the stripping of the contaminant peaks. As mentioned earlier, the natural background accumulated in the sum mode window at the rate of 0.469 counts/sec. Beam induced counts accumulated at rates of 0.183 and 0.086 counts/second for the 1000 and 850 keV runs, respectively, for average He^{+} beam currents of 20 uamperes. The majority of the counts therefore came from natural background, and it is to be anticipated that the corrected spectra will show wide fluxuations due to the counting statistics.

Although the contaminant peaks could not be clearly discerned, the spectral shapes were known for each expected source of counts in the quartz, and the shapes differed greatly in different regions of the spectrum. This suggested dividing the

energy region above 3.2 MeV (below which the two spectra were totally useless) into three large regions, and considering the contributions of each source to each of the three regions. The sources considered were neutrons, the 3.85 MeV gamma from $^{10}B(\alpha,p_3\gamma)^{13}C$, and whatever $^{16}O(\alpha,\gamma)^{20}Ne$ yield might be present. Although the possibility of α-capture on the silicon in the target should be considered in principle, it was eliminated on the basis of the high Coulomb barrier for the reaction.

The neutron response of the detectors was available from the spectra measured for $^{13}C(\alpha,n)^{16}O$ at 1000 and 850 keV. Different reactions, such as $^{10,11}B(\alpha,n)^{13,14}N$ would have contributed neutrons of somewhat different energy than the neutrons from carbon contamination, but the shape of the neutron response varied slowly above 3 MeV, and should have been relatively independent of the expected neutron energy differences. Therefore, the $^{13}C(\alpha,n)^{16}O$ spectra were used to represent the shape of all the neutron response curves.

The shape of the 3.85 MeV gamma from $^{10}B(\alpha,p_3\gamma)^{13}C$ had been measured at 1000 keV on a boron target, as mentioned before. It had also been measured at 850 keV, but at this energy, contributions from neutrons were clearly evident. Since the neutron shape was already accounted for, the shape of the $^{10}B+\alpha$ spectrum at 1000 keV was used for both runs.

The spectrum shape due to $^{16}O(\alpha,\gamma)^{20}Ne$ yield was estimated by correcting the 1319 keV spectrum for the small change in

excitation energies. This is a reasonable procedure, since any other levels in ^{20}Ne at these low energies would be expected to exhibit decay structures very similar to that of the 1319 keV resonance.

The borders for the three regions are indicated by the numbered arrows on the abscissa of Figure 16. Regions 1, 2, and 3 spanned the energy ranges 3.1-4.2 MeV (arrow 1 to arrow 2), 4.2-6.4 MeV (arrow 2 to arrow 3), and 6.4-8 MeV (arrow 3 to the end of the spectrum), respectively. This selection of regions provided the highest sensitivity to the shape differences of the contaminant and oxygen yields, and therefore used most efficiently whatever information was available in the quartz target spectrum. The neutron shape was quite flat, and decreased slowly through each region; the 3.85 MeV gamma from boron contamination contributed mainly to region 1; and the yield from $^{16}O(\alpha,\gamma)^{20}Ne$ could have contributed only to regions 1 and 2.

The following analysis was then applied, independently, to both the 850 and 1000 keV quartz spectra. For region 1, the quartz yield, N(1) (corrected for natural background), was expressed as the sum of the absolute contributions from neutrons, the boron γ ray, and $^{16}O(\alpha,\gamma)^{20}Ne$:

$$(\text{neutrons}) + (\text{boron}) + (\text{oxygen}) = (\text{quartz}).$$

Each absolute contribution was then expressed as the product of the number of counts in region 1 of the corresponding shape

spectrum, C(1), B(1), and O(1), and an unknown coefficient, X_i, that normalized each shape contribution to its actual contribution to the quartz spectrum,

$$X_C C(1) + X_B B(1) + X_O O(1) = N(1). \qquad (27a)$$

Two similar expressions followed immediately,

$$X_C C(2) + X_B B(2) + X_O O(2) = N(2)$$
$$X_C C(3) + X_B B(3) + X_O O(3) = N(3) \qquad (27b,c)$$

where the same set of X_i apply for each region of the spectrum. As expected from the discussion of the last paragraph, O(3) and B(3) were quite small compared to O(1) and B(1), respectively. Note that the shape spectra do not need to be normalized to an absolute yield, since the normalization can be absorbed in the X_i. The goal of the analysis was to determine the product, $X_O O(1+2)$, for this represented the yield in the SCA window from $^{16}O(\alpha,\gamma)^{20}Ne$, which could be compared directly with the yield from the 1319 keV resonance.

Equation 27 was coded in the matrix form, $\underline{A}\,\underline{X} = \underline{N}$, where $\underline{A}$ is the shape matrix, $\underline{N}$ is the quartz yield vector for the spectrum, and the vector $\underline{X}$ has components X_C, X_B, and X_O. The Caltech-IBM 360-50 computer then calculated the inverse of $\underline{A}$ and determined the solution for $\underline{X}$, for both the 850 and 1000 keV runs. The errors in $\underline{X}$ are of major importance to

the determination of an upper limit on the yield. An expression for the error vector, $\underline{\sigma_X}$, can be obtained by letting $\underline{A}$ and $\underline{N}$ change incrementally, and demanding that $\underline{X}$ change in such a way that the matrix equation is still satisfied, becoming

$$(\underline{A} + \underline{dA})(\underline{X} + \underline{dX}) = (\underline{N} + \underline{dN}). \tag{28}$$

Expanding, discarding the second order term, $\underline{dAdX}$, and subtracting the original matrix equation, one obtains

$$\underline{dX} = \underline{A}^{-1}(\underline{dN} - \underline{dA}\,\underline{X}) . \tag{29}$$

By replacing the increments with the known uncertainties in $\underline{A}$ and $\underline{N}$, adding up the coefficients of each uncertainty linearly, and summing the resulting independent terms quadratically, the $\underline{\sigma_X}$ vector was obtained. Finally, the solutions for the oxygen contribution in the SCA window were 659 ± 571 and 172 ± 348 counts, respectively, for the 1000 and 850 keV runs, for total integrated He^+ currents of 0.46 and 0.36 Coulombs.

The fact that the answer for the 1000 keV run was not quite compatible with zero was cause for some concern. However, the previously neglected $^{7}Li(\alpha,\gamma)^{11}B$ resonance at 958 keV must have been responsible for some of the counts. Although the excitation in ^{11}B is 9.27 MeV, the level decays 67% through the level at 4.44 MeV, yielding two γ rays, of energies 4.44 and 4.83 MeV. For the broad regions considered in this analysis, the spectrum

shape from these gammas would be represented fairly well by the $^{16}O(\alpha,\gamma)^{20}Ne$ shape, and so yield from $^{7}Li(\alpha,\gamma)^{11}B$ could have resulted in an overestimate of the oxygen yield. Using the lithium concentration quoted by the manufacturer, the literature value for the strength of the 958 keV resonance (Ajzenberg-Selove and Lauritsen, 1966), Equation 6, and the NaI detection efficiencies, the yield from ^{7}Li contamination was estimated to be 1000 ± 550 counts. For the purpose of calculating an upper limit, 450 counts were attributed to lithium and subtracted from the 1000 keV solution, leaving 209 ± 571 net counts, which is compatible with zero.

To convert the results to an upper limit on the strength, the uncertainty was added to the net counts; this result was compared with appropriate corrections for the differences in energy and in integrated beam current, and then normalized to the 1319 keV resonance strength, 18.1 meV. For example, for 1000 keV, the limit was calculated in the following way:

$$(2J+1)(\Gamma_\alpha\Gamma_\gamma/\Gamma)_{lab} < (18.1 \text{ meV}) \frac{(0.061 \text{ C})(1000 \text{ keV max.})(780 \text{ counts})}{(0.464 \text{ C})(1319 \text{ keV})(31900 \text{ counts})}$$

$$< 0.044 \text{ meV}.$$

A useful independent check was available for the 1000 keV analysis. Because the $^{10}B(\alpha,p_3\gamma)^{13}C$ resonance at 1510 keV had been measured with both a boron target and the

evaporated quartz target, the amount of boron in the quartz target could be calculated by comparing the yields from the two targets. This allowed a direct calculation of X_B for the 1000 keV run. The result was $X_B = 0.16 \pm 15\%$; the value obtained from the matrix analysis was $X_B = 0.157 \pm 23\%$.

E. Yield for $E_{He^+} < 1000$ keV: 2. Coincidence Results

By monitoring the coincident detection of both members of the γ_1 transition expected from any level in ^{20}Ne, it was anticipated that the ratio of beam induced count rate to natural background count rate could be dramatically increased. The efficiency for coincident detection was estimated to be roughly a factor of 20 lower than the sum mode detection efficiency, but, if the natural background could produce only random coincidences, then, with a background rate in the upper and lower coincidence windows of 0.32 and 1.9 counts per second, and a resolving time of 1 μsecond (twice the duration of the logic pulses), the random rate should have been ≈0.61 counts per 10^6 seconds. In practice, however, the background coincidence rate was measured to be 3.56 ± 0.22 counts per 10^3 seconds, indicating probably that two or more members of a cosmic ray shower were being detected, or that an energetic charged particle at a fairly large zenith angle was traversing both NaI

crystals. In order to measure the true random rate, a delay line of arbitrary length longer than the resolving time was inserted between one SCA and its coincidence input. This circuit ran for a week ($\approx 0.6 \times 10^6$ seconds) without registering a count.

In order to decrease the background coincidence rate, four paddles of plastic scintillator, each 50 cm by 50 cm by 1 inch thick, and having its own phototube, were mounted outside the lead shielding, and run in anticoincidence with the NaI coincidence pulses. Although a more efficient geometry for cosmic ray anticoincidence would have the anticoincidence shield inside the lead shielding, this would have involved considerable cost and effort.

The plastic shields were checked for uniformity of response with an ^{88}Y source, and the gains were matched by varying the phototube high voltage supply and observing the spectra of various sources. The four anode signals were summed resistively and DC coupled to four Hewlett-Packard wide-band distributed amplifiers in series. The fast output signal was inspected with a tunnel diode discriminator (leading edge timing), and the slow logic output pulse (0.3 useconds wide) from the discriminator was stretched and delayed to match the timing requirements of the NaI spectrometer coincidence system, which used cross-over timing. The system timing was carefully inspected before each run, using a pulse generator and an

oscilloscope. In order to veto as many background pulses as possible, the discriminator threshold was set very low, passing all pulses higher than ~200 mV, corresponding to roughly 300 keV of energy deposited in the plastic scintillator. The only reason for the use of leading edge timing in the veto system was the superior stability at very low thresholds of the tunnel diode discriminator over the conventional Schmitt trigger discriminator. The threshold was kept high enough so that the dead time due to veto pulses was always less than 3%.

The anticoincidence shields reduced the background rate from 3.56 to 1.17 ± 0.13 counts/10^3 seconds.

Coincidence data and sum mode data were gathered at the same time. As for the 2490 keV resonance, a second SCA, the > 1.6 window, was set for the region just above the 1.6 MeV window to monitor the background. The background coincidence rate in this window was 0.548 ± 0.129 counts/10^3 seconds. Coincidence datawere also obtained during the runs in which the $^{10}B(\alpha,p_3\gamma)^{13}C$ and $^{13}C(\alpha,n)^{16}O$ spectra were measured. For each case, the > 1.6 coincidence pair registered fewer counts than the 1.6 pair.

With these data available, the net counts attributable to $^{16}O(\alpha,\gamma)^{20}Ne$ in the coincidence system were calculated in two ways. The first way depended on the results of the previously described matrix analysis. Using the same set of

X_1, and the coincidence information from boron and carbon runs, corrections were calculated for the quartz coincidence yield. For the 1000 keV work, the raw quartz data, and the natural background, boron, and carbon corrections combined as follows (the errors are statistical):

	1.6 Coincidence	> 1.6 Coincidence
Quartz	24 ± 4.9	20 ± 4.5
Natural Background	11 ± 1.2	5 ± 1.2
Boron	3 ± 0.9	2 ± 0.6
Carbon	14 ± 1.6	11 ± 1.4
Net	-4 ± 5.4 counts	2 ± 4.9 counts

The second method was independent of the matrix analysis, and therefore perhaps preferred. Since, for all sources, the > 1.6 pair registered fewer counts than the 1.6 pair, a simple subtraction of the > 1.6 data from the 1.6 data also yielded an upper limit. The contribution from natural background was removed because its calculation was straightforward. For 1000 keV again, using the above data for quartz and natural background, the corrected 1.6 value was 13 ± 5.0 counts, and the > 1.6 value was 15 ± 4.6 counts. The difference of these values was -2 ± 6.8 counts.

Similar calculations were carried out for the 850 keV

data, yielding, in each case, an answer compatible with zero. The number used for the upper limit was the net counts plus the uncertainty, for positive net counts, and just the uncertainty for negative net counts. These numbers were converted to upper limits for $(2J+1)\Gamma_\alpha\Gamma_{\gamma_1}/\Gamma$ by comparing with the coincidence yield from the 1116 keV resonance, just as the sum mode counts were compared with the 1319 keV resonance yield. The results for all of the $^{16}O(\alpha,\gamma)^{20}Ne$ strengths appear in Table 3.

TABLE 3: Resonance Strengths for $^{16}O(\alpha,\gamma)^{20}Ne$

Resonance Energy (keV)[a]	$(2J+1)\Gamma_\alpha\Gamma_\gamma/\Gamma$ (meV)[a]	$(2J+1)\Gamma_\alpha\Gamma_{\gamma_1}/\Gamma$ (meV)[a]
2490	41 $\pm$ 12	
1319	18.2 $\pm$ 3.6	
1116	1.9 $\pm$ 0.38	
<1000	$\leq$ 0.044	$\leq$ 0.031
< 850	$\leq$ 0.036	$\leq$ 0.024

[a]The energies and strengths are given in laboratory units.

VII. ASTROPHYSICAL RESULTS

A. $^{28}Si(\alpha,\gamma)^{32}S$

The astrophysical interaction rate, $\langle\sigma v\rangle$, for this reaction was calculated using Equation 2, Section IB; the values are tabulated in Table 4 for various temperatures. It should be pointed out that the rate expressed in Equation 2 considers α-capture only on ^{28}Si in its ground state. For $T_9 = 5$ (T_9 is the temperature in units of 10^9 °K), approximately 7.4% of the ^{28}Si nuclei will be found in the first excited state; therefore, α-capture on this state could make a contribution to the total interaction rate of ^{28}Si. It follows that the photodisintegration lifetime of ^{32}S through α channels could be similarly shortened. Unfortunately, particle capture on an excited state cannot be studied directly in the laboratory; therefore, the effects of excited states on the interaction rate can only be estimated from calculations. An example of such a calculation for the cases of $^{27}Al+p$ and $^{24}Mg+\alpha$ is given by PBL.

For the calculation of the interaction rate, the $^{28}Si(\alpha,\gamma)^{32}S$ data measured here were supplemented by data from Smulders (1964) and Langevin et al. (1965); the supplemental data are given in Table 5. As mentioned in the introduction, Smulders measured the partial resonance strengths, $(2J+1)\Gamma_\alpha\Gamma_{\gamma_0+\gamma_1}/\Gamma$, only, for four resonances; the strength for the resonance at the lowest

TABLE 4: The Stellar Interaction Rate for $^{28}Si(\alpha,\gamma)^{32}S$

Temperature (10^9 °K)	$N_A\langle\sigma v\rangle$ (sec^{-1})
0.3	2.43×10^{-23}
0.4	5.32×10^{-17}
0.5	3.16×10^{-13}
0.6	9.93×10^{-11}
0.7	5.87×10^{-9}
0.8	1.23×10^{-7}
0.9	1.30×10^{-6}
1.0	8.59×10^{-6}
1.5	2.64×10^{-3}
2.0	5.68×10^{-2}
2.5	4.12×10^{-1}
3.0	1.63
3.5	4.44
4.0	9.46
4.5	17.0
5.0	27.1

TABLE 5: Supplemental Resonance Data for $^{28}Si(\alpha,\gamma)^{32}S$

Resonance Energy (keV)[a]	$(2J+1)\Gamma_\alpha\Gamma_\gamma/\Gamma$ (eV)	Source
2878 ± 4	0.75 ± 50%	Smulders (1964)
2904 "	1.31 "	"
3162 "	0.37 "	"
3413 ± 6	0.15 ± (x 2)	Langevin et al. (1965)
3616 "	0.17 "	"
3753 "	1.0 "	"
3834 "	0.38 "	"
3879 "	0.43 "	"
3993 "	0.43 "	"
4096 "	0.24 "	"
4210 "	0.62 "	"
4298 "	1.8 "	"

energy, 2618 keV, was measured here, and this value was used to normalize the partial strengths of the other three resonances at higher energies, measured by Smulders. This estimate of the total strengths for these resonances was assigned an uncertainty of 50%.

Although Langevin did not calculate strengths for the resonances that he found, he provided a diagram of the excitation functions. Because the target he used contained natural silicon, resonances in $^{30}Si(\alpha,\gamma)^{34}S$ also appeared in his excitation functions. The strengths for three of these resonances had been measured by McMurray and Van Heerden (1965), which, with knowledge of the natural abundances of the silicon isotopes, provided a factor with which the peak heights for the $^{28}Si(\alpha,\gamma)^{32}S$ resonances in Langevin's excitation function could be converted into strengths. The three $^{30}Si(\alpha,\gamma)^{34}S$ resonances provided three values for this factor; the values were consistent. Clearly this procedure could introduce large errors, so the strength estimates must be assigned an uncertainty of at least a factor of two.

The contributions from the various data to the interaction rate are compared in Table 6, which illustrates the importance of the new data measured here.

Photodisintegration rates were calculated with Equation 3, Section IB, and the results are listed in Table 7. Again, the

TABLE 6: Comparison of Contributions to the Interaction Rate for $^{28}Si(\alpha,\gamma)^{32}S$

Temperature (10^9 °K)	Fraction of Interaction Rate Due to: 1776 keV Resonance	All Resonances, This Experiment	Resonances from Smulders[a]	Resonances from Langevin[b]
0.5	99%	100%	———	———
1.0	87	100	———	———
2.0	38.5	88.3	11.4%	0.3%
3.0	14.7	67.9	29.8	2.2
4.0	7.4	54.3	39.3	6.3
5.0	4.5	45.5	43.1	11.2

[a,b]The contributions listed in these columns were normalized by methods discussed in the text.

TABLE 7: ^{28}Si Photodisintegration Rates (α_0 Channel)

Temperature (10^9 °K)	$\lambda_{\gamma,\alpha}$ (seconds^{-1})
0.5	7.93×10^{-74}
1.0	6.48×10^{-31}
2.0	3.91×10^{-9}
3.0	1.44×10^{-1}
4.0	1.08×10^{3}
5.0	2.42×10^{5}

contributions from excited states in ^{28}Si are ignored. Comparison of the photodisintegration rates for the α and p channels indicates that the α channel dominates for $T_9 < 2$; the p channel becomes important at higher temperatures. The p channel rate was calculated with data from the Endt and Van der Leun compilation (1967) for the $^{31}P(p,\gamma)^{32}S$ reaction; differences in the reported data show the need for further investigation.

The upper limits listed in Table 2 for resonance strengths below 1400 keV show that no undetected low-energy resonance can contribute appreciably to $\langle \sigma v \rangle$ for $T_9 \geq 2$. The contribution from a 1400 keV resonance of strength 0.0008 eV would be 18% of the 1776 keV resonance contribution. To equal the 1776 contribution, a resonance of strength 0.0001 eV must

lie below 660 keV, implying a width Γ_α several orders of magnitude greater than the Wigner limit, for this energy.

Two and four parameter fits to the interaction rates as a function of temperature are provided to facilitate astrophysical calculations. The formula, $N_A\langle\sigma v\rangle = 9.36\times10^{2}\exp(-18.8/T_9)$ fitted the data to within 30% for $T_9 = 1-5$, but was low by a factor of 7.4 at $T_9 = 0.5$. The form, $N_A\langle\sigma v\rangle = 2.73\times10^{2}\exp(-17.1/T_9) + 2.81\times10^{3}\exp(-24.9/T_9)$ fitted the data to within 8% over the range $T_9 = 0.5-5$. It should be remarked that the experimental uncertainty in the data is much greater than 8%.

B. $^{16}O(\alpha,\gamma)^{20}Ne$

The resonance strengths measured for this reaction agree with those measured by Van der Leun et al. (1965), and no evidence was found for resonances at lower energies; therefore the situation for helium burning is unchanged.

Typical α energies at helium burning temperatures are far below the energies of the three lowest resonances in $^{16}O(\alpha,\gamma)^{20}Ne$; at the low stellar energies, Γ_α will have changed markedly from its value at the resonance energy, because of the decrease in the penetration factor. Equation 2 therefore is no longer valid. Clayton (1968) has discussed in detail the appropriate formulas for calculating the interaction rates in these circumstances. Fowler, Caughlan, and Zimmerman (1967), have given an expression for

the nonresonant rate for this reaction which should be accurate to within a factor of 3 for $T_9 < 0.2$,

$$N_A\langle\sigma v\rangle = 1.34\times10^9(1 + 1.05\times10^{-2}T_9^{1/3})\ T_9^{2/3}\exp(-39.76/T_9^{1/3}).$$

The results of the present measurements do not affect this expression.

The hypothesis proposed by Asano and Sugimoto (discussed in Section IA) receives no support from this work, although it was a priori unlikely that $^{16}O(\alpha,\gamma)^{20}Ne$ could have been of much help anyway. Asano and Sugimoto calculated the rate of energy generation by the $^{14}N(\alpha,\gamma)^{18}F$ reaction in the core, using a formula for the reaction rate given by Reeves (1965). Later experimental data on the reaction show this rate to be far too high. One can propose the following argument concerning energy generation by $^{16}O(\alpha,\gamma)^{20}Ne$. Assume that a resonance exists somewhere below 850 keV, having a strength equal to the upper limit determined in the present work. Assume also that the ratio of the ^{16}O concentration to the ^{14}N concentration after CNO burning at, say, $T_9 = 0.1$, is 0.003 (Clayton, 1968). Then calculate how low the energy of the assumed resonance must be for the reaction to generate energy at 1% of the rate calculated by Asano and Sugimoto (with the old $^{14}N(\alpha,\gamma)^{18}F$ data). The answer, for the assumed resonance strength, is $E_{r,CM} = 306$ keV. A simple penetration factor calculation shows that a resonance of this strength, at this energy, must have a value for Γ_α that is a factor of 10^4

greater than the Wigner single-particle limit (or $\theta_\alpha^2 = 10^4$). It can therefore be safely stated that the $^{16}O(\alpha,\gamma)^{20}Ne$ reaction can not supply the energy needed for igniting a helium flash in the Asano-Sugimoto model.

VIII. EXPERIMENTAL CONCLUSIONS

Both the $^{16}O(\alpha,\gamma)^{20}Ne$ and $^{28}Si(\alpha,\gamma)^{32}S$ reactions were investigated in energy regions where the reaction yield was very low. Some of the background problems encountered in this experimental situation will be discussed. As the problems were somewhat different for different He^+ energies, two energy ranges will be treated separately.

A. Incident Energies Between 1 - 3 MeV

In this energy range, weak resonances having strengths $(2J+1)\Gamma_\alpha\Gamma_\gamma/\Gamma \approx 20 - 100$ meV were studied. The main source of background was from beam dependent (α,n) reactions on contaminants in and on the target. A list of the reactions and resonances encountered appears in Table 1. Alpha-capture reactions were also probably present, but at this yield level, they did not become important.

Clearly, very high purity targets would be required for further similar studies, and any steps taken to prevent carbon buildup or target oxidation would prove valuable. The use of time-of-flight techniques with a pulsed beam would eliminate many neutron counts and natural background counts from the spectrum, but such techniques would also impair the gamma counting rate. A Ge(Li) detector could provide help in identifying contaminant

reactions; it is also necessary to know the features of α-induced reactions on the contaminants found.

The coincidence technique proved to be very valuable in identifying yield with the reaction of interest. A 2-dimensional analysis system, or at least another battery of single channel analyzers and coincidence gates, would provide the capability for monitoring other transitions, which would allow a more positive identification, and at the same time, provide some information about relative transition strengths. A single window examining only the high energy region of the spectrum may miss some astrophysically important resonances.

Although more beam or a higher detection efficiency would allow shorter runs, the contaminant background is beam dependent, and would not be reduced by these means.

B. Incident Energies Below 1 MeV

This region is below the energies of most resonances in particle reactions, such as (α,n) reactions, so yield from these reactions would be non-resonant in nature, and would therefore vary slowly with energy. The strengths typically of interest in this region are of the order of 0 - 2 meV; it is often desired to put as low an upper limit as possible on the yield. Some contaminant alpha capture reactions can compete with such low yields, for example, the $^{7}Li(\alpha,\gamma)^{11}B$ reaction

discussed in Section VII D.

The main contribution to the background, however, was from natural background, which accumulated 3 - 5 times faster than beam induced yield. This situation could be improved by either increasing the beam dependent yield or reducing the natural background, as discussed below.

Incorporating larger detectors could at most increase the yield by a factor of 2 or 3, and the larger detector volume would very likely increase the natural background rate at the same time. The larger detector might also have poorer resolution.

Increasing the beam current would help, provided that the target could withstand it, and the accelerator could supply it.

Probably a more profitable approach would be to redesign the anticoincidence system and shielding so that the natural background rate is reduced. An obvious step would be to construct an anticoincidence shield inside the lead. At low energies, ^{40}K (1.49 MeV) and ThC" (2.61 MeV) would still be a problem unless the anticoincidence shield was thick enough to efficiently veto these gamma rays.

D. Other Reactions

The partial detection efficiency method has now been applied to the study of two product nuclei: ^{28}Si and ^{32}S. For other, similar reactions, it should be possible to check the η curves fairly easily by a study of the proton-capture reactions forming

the nucleus in question, and to apply the result to the study of alpha-capture into the same nucleus. Branching ratios for states excited by proton-capture have been measured for many nuclei having $A \leq 40$, and are available in the literature.

REFERENCES

F. Ajzenberg-Selove and T. Lauritsen, 1959, Nucl. Phys. 11, 1.

F. Ajzenberg-Selove and T. Lauritsen, 1966, Nucl. Phys. 78, 1.

F. Ajzenberg-Selove and T. Lauritsen, 1968, Nucl. Phys. A114, 1.

W. D. Arnett, 1969, Ap. J. 157, 1369.

N. Asano and D. Sugimoto, 1968, Ap. J. 154, 1127.

D. Bodansky, D. D. Clayton, and W. A. Fowler, 1968, Astrophys. J. Suppl. No. 148, 16, 299.

T. W. Bonner, A. A. Kraus, Jr., J. B. Marion, and J. P. Schiffer, 1956, Phys. Rev. 102, 1348.

E. M. Burbidge, G. R. Burbidge, W. A. Fowler, and F. Hoyle, 1957, Rev. Mod. Phys. 29, 547

D. Clayton, 1968, Principles of Stellar Evolution and Nucleosynthesis, McGraw-Hill, New York.

P. M. Endt and C. Van der Leun, 1962, Nucl. Phys. 34, 1.

P. M. Endt and C. Van der Leun, 1967, Nucl. Phys. A105, 1.

J. Faulkner, 1966, Ap. J. 144, 978.

W. A. Fowler, G. R. Caughlan, and B. A. Zimmerman, 1967, Ann. Rev. Astr. and Astrophys. 5, 525.

W. A. Fowler and F. Hoyle, 1964, Astrophys. J. Suppl. No. 91, 9, 201.

W. A. Fowler, 1969, private communication.

A. Gallmann, F. Hibou, and P. Fintz, 1969, Nucl. Phys. A123, 27.

H. E. Gove, 1959, Nuclear Reactions I, ed. by P. M. Endt and M. Demeur, North Holland Publishing Company, Amsterdam, Ch. VI.

H. E. Gove, A. E. Litherland, and M. A. Clark, 1961, Proc. Rutherford Jubilee International Conference,ed. by J. B. Birks; Heywood and Co., London, 787.

G. W. Grodstein, 1957, X-Ray Attenuation Coefficients from 10 keV to 100 MeV, National Bureau of Standards Circular 583.

Harshaw Chemical Company, 1962, Harshaw Scintillation Phosphors, Cleveland, Ohio.

C. Hayashi, R. Hoshi, and D. Sugimoto, 1968, Progr. Theoret. Phys. Suppl. No. 222.

J. A. Kuehner, 1961, Proc. Rutherford Jubilee International Conference, ed. by J. B. Birks; Heywood and Co., London, 787.

M. Langevin, H. Laurent, and J. Vernotte, 1965, C. R. Acad. Sc. Paris, t. 261, 4055.

P. B. Lyons, 1969, Ph. D. Thesis, California Institute of Technology (referred to as PBL).

P. B. Lyons, J. W. Toevs, and D. G. Sargood, 1969, Nucl. Phys. A130, 1 (referred to as LTS).

W. R. McMurray and I. J. Van Heerden, 1965, Nucl. Phys. 72, 113.

J. H. Neiler and P. R. Bell, 1965, Alpha-, Beta-, and Gamma-Ray Spectroscopy, ed. by K. Siegbahn, North-Holland Publishing Co., Amsterdam, Ch. V.

J. W. Olness and E. K. Warburton, 1967, Phys. Rev. 156, 1145.

P. D. Parker, 1968, Phys. Rev. 173, 1021.

J. D. Pearson, 1963, Ph. D. Thesis, California Institute of Technology.

M. E. Rose, 1953, Phys. Rev. 91, 610.

M. E. Rose, 1957, Elementary Theory of Angular Momentum, John Wiley and Sons, New York.

H. Reeves, 1965, in Stars and Stellar Systems, Vol. 8: Stellar Structure, ed. by L. H. Aller and D. B. McLaughlin, Univ. of Chicago Press, Chicago, 113.

P. J. M. Smulders, 1964, Physica 30, 1197.

P. J. M. Smulders, 1965, Physica 31, 973.

J. W. Truran and W. D. Arnett, 1969, Nucleosynthesis in Explosive Oxygen Burning (to be published).

J. W. Truran, W. D. Arnett, and A. G. W. Cameron, 1967, Can. J. Phys. 45, 2315.

J. W. Truran, A. G. W. Cameron, and A. Gilbert, 1966, Can. J. Phys. 44, 563.

C. Van der Leun, D. M. Sheppard, and P. J. M. Smulders, 1965, Phys. Lett. 18, 134 (referred to as VSS).

R. V. Wagoner, 1969, Astrophys. J. Suppl. No. 162, 18, 247.

W. Whaling, 1958, Handbuch der Physik 34, 193.

C. Williamson and J. P. Boujot, 1962, Commissariat à l'Energie Atomique Report CEA-2189.